# Lattice dynamics and phonon characteristics of complex perovskite microwave ceramics

*Feng Shi[1] ✉, He-Lei Dong[2,3], Di Zhou[4], Chun-Hai Wang[5], Qiu-Lin Tan[2,3], Ji-Jun Xiong[3], Qing Wang[6]*

[1]*School of Material Science and Engineering, Shandong University of Science and Technology, Qingdao, 266590, People's Republic of China*
[2]*School of Instrument and Electronics, North University of China, No. 38 Xueyuan Road, Tai Yuan, 030051, People's Republic of China*
[3]*Science and Technology on Electronic Test and Measurement Laboratory, North University of China, No. 38 Xueyuan Road, Taiyuan 030051, People's Republic of China*
[4]*Electronic Materials Research Laboratory, Key Laboratory of the Ministry of Education and International Center for Dielectric Research, Xi'an Jiaotong University, Xi'an, 710049, Shan'xi, People's Republic of China*
[5]*Academy for Advanced Interdisciplinary Studies, Southern University of Science and Technology, Shenzhen 518055, People's Republic of China*
[6]*School of Civil Engineering and Architecture, Shandong University of Science and Technology, Qingdao, 266590, People's Republic of China*
✉ *E-mail: sf751106@sina.com.cn*

**Abstract:** Complex perovskite microwave dielectric ceramics (MWDCs) of $A(B'_{1/3}B''_{2/3})O_3$-type ($A$ = Ba, Sr,…; $B'$ = Mg, Zn,…; $B''$ = Nb, Ta), which exhibit excellent dielectric properties, have currently been widely used in microwave and millimetre wave devices. Vibrational spectra, including both Raman and far-infrared (FIR) spectra, are powerful tools to investigate the atomic thermal vibrational properties of MWDCs and reveal the intrinsic origin of dielectric properties. In this review, lattice dynamics and phonon characteristics of the $A(B'_{1/3}B''_{2/3})O_3$-type MWDCs are summarised and presented in detail to introduce remarkable progress in this field and make a guide for the design of novel advanced MWDCs. The atomic sites and the corresponding modes in Raman and FIR spectra are identified and illuminated. The effects of the processing conditions and the ordered superstructures in the nanoscale region on vibrational modes are summarised systemically. Intrinsic properties can be extrapolated from the fitting results of FIR spectroscopy, which were also discussed based on the Kramers–Krönig relations, Lorentz three-parameter classical model and four-parameter semi-quantum model. The correlations between vibrational modes (phonons), crystal structures, and dielectric properties are created, which can help to build the mathematical models so as to understand the structure–property relationship of MWDCs better.

## 1 Introduction

Nowadays, wireless communication systems have stepped into the microwave and millimetre (MW, 300 MHz–3000 GHz) frequency range, where advanced functional ceramic materials are usually served as capacitors, substrates, and filters in wireless telecommunication devices [1–4]. Generally, dielectric materials used in these devices are called microwave dielectric ceramics (MWDCs), which usually present appropriate dielectric constants ($\varepsilon_r$), high-quality factors ($Q \times f$), and near zero temperature coefficient of resonant frequencies (TCF/$\tau_f$). The applications of ceramic materials in various microwave components accelerate further considerable miniaturisation of communication devices, which requires high-dielectric constants (because there is an inverse relationship between the size of resonators and $\sqrt{\varepsilon_r}$, i.e. the materials with high-dielectric constants are preferable due to the benefit of size reduction) with a small or zero TCF (<±10 ppm/°C). Moreover, MWDCs with high-$Q$ factor are required for the resonators and filters with high performance [5–10].

The concept of the dielectric resonator was put forward by Richtmyer in 1939 [11] and it offers superiority in minimisation and signal selectivity compared with the traditional materials. By now, a series of MWDCs with a range of permittivities have been developed as follows: (i) (Mg,Zn)TiO$_3$, for $\varepsilon_r \sim 20$, (ii) $A(B'_{1/3}B''_{2/3})O_3$-type ($A$ = Ba, Sr; $B'$ = Mg, Zn,…; $B''$ = Nb, Ta), for $\varepsilon_r \sim 30$–40, (iii) (Sr,Ca)TiO$_3$–(La,Nd)AlO$_3$, BaTi$_4$O$_9$, and Ba$_2$Ti$_9$O$_{20}$, for $\varepsilon_r \sim 40$–45, (v) BaO–Ln$_2$O$_3$–TiO$_2$ (Ln = La, Nb, Sm) for $\varepsilon_r >$ 70, etc. [12–27]. Among these MWDCs, the $A(B'_{1/3}B''_{2/3})O_3$-type complex perovskite ceramics has two different oxidation state elements on the B-sites, i.e. $B'$ (divalent) and $B''$ (pentavalent) ions. Generally, the B-sites that are located in the centre of oxygen octahedron are occupied by the transition metal ions and

surrounded by larger A-site ions. The multiple cation substitutions for either A/B sites, or both, form the complex perovskites. Owing to the principles of chemistry, the complex perovskite ceramics with the $A(B'_{1/3}B''_{2/3})O_3$ formula can form numerous compounds with different dielectric properties, combined ionic radius, tolerance factor, valence etc. [28].

The ideal ABO$_3$ perovskite ceramic has a cubic structure with a space group of *Pm3m* and it is made up of a three-dimensional (3D) network of corner-sharing BO$_6$ octahedral, with the A-site cation filling the 12 coordinated cavities, i.e. cuboctahedral holes. The classic standard cubic perovskite structure is observed in SrTiO$_3$. The Ti$^{4+}$ ions are placed at the corners, and the Sr$^{2+}$ ions are at the centre of the cubes, and the O$^{2-}$ ions are at the centres of the 12 cube edges, giving corner-shared strings of TiO$_6$ octahedral [29]. The ABO$_3$ perovskite structure is very flexible and can accommodate most of the metallic elements in the periodic table [30]. Another description is in terms of the close packing of A and O ions such that the AO$_3$ layers are stacked one over the other. Thus, when the stacking of the AO$_3$ layers is cubic, the B cation octahedral sharing all corners can form the ideal perovskite structure [31–34].

Based on the ionic radii in A/B sites, the substitution in the A and B sites can cause tilting of the oxygen octahedron, which reduces the volume of the cuboctahedron until it adapts the size of the A cations and generates several ordered perovskite structures [32, 33]. Fig. 1 shows the crystal structure of the Ba(Mg$_{1/3}$Ta$_{2/3}$)O$_3$ (BMT) as an example. The small spheres, medium spheres, and large spheres denote oxygen atoms, Mg/Ta atoms in [TaO$_6$] octahedron, and Ba atoms, respectively, and the B cations occupy the octahedral holes.
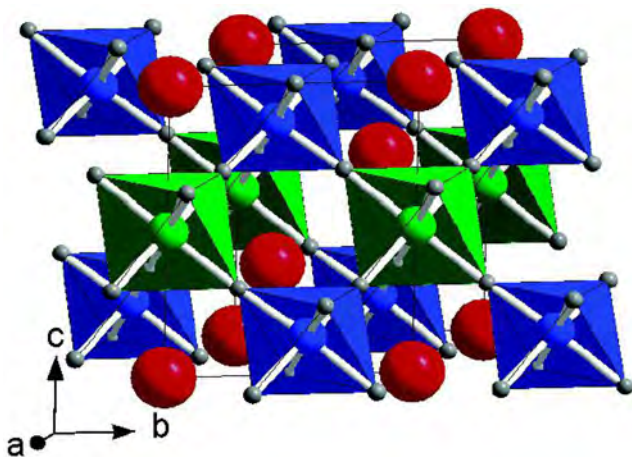
**Fig. 1** *Crystal structure of ordered BMT [35]*

Tilting of an octahedron ($BO_6$) reduces the symmetry of the structure [30]. As a result, dielectric properties can be modified by adjusting the degree of tilting of $BO_6$ octahedron [36], whose existence in the $Ba_{1-x}Sr_x(Mg_{1/3}Ta_{2/3})O_3$ (BSMT) ceramics was first verified by Nagai *et al.* [37], and the octahedral tilting in simple cubic perovskite was also investigated by Glazer [38] and Aleksandrov [39]. Furthermore, the correlation between $\tau_f$ and octahedral tilting was studied by Reaney *et al.* [40] in the Ba- and Sr-based 1:2 ordered complex perovskite ceramics. Subsequently, new models were developed by Nagai *et al.* [41] to study the octahedral tilting in the 1:2 ordered structures. Two regions in $Ba_{1-x}Sr_x(Mg_{1/3}Nb_{2/3})O_3$ (BSMN) ceramics were recognised by Lee *et al.* [37, 42]: the 1:2 ordered trigonal structures without/with octahedral tilting [43].

The B-site ordering is remarkably influenced by ionic radius and electrovalence of *B′* and *B″* cations. Depending on the differences of ionic radius and electrovalence between the *B′* and *B″* cations, these compounds can adapt ordered or disordered structures. Particularly, the complex perovskites with non-ideal A–O and B–O bond distances and distorted non-cubic symmetries are meaningful in future microwave communication development in high-frequency communication. The ordering leads to a trigonal unit cell whose *c*-axis is along the $\langle 111 \rangle$ direction of the original perovskite with a *B′–B″–B″–B′…* layer sequence, which is called long-range ordering (LRO). The corresponding unit-cell parameters are $a \simeq 2\sqrt{a_c}$ and $c \simeq \sqrt{3}a_c$, and the space group subsequently changes to $P\bar{3}m1(D_{3d}^3,$ trigonal quasi-layered structure). In the study of Takahashi *et al.* [44], four possible 1:2 ordered models for BMT with space groups, $P\bar{3}m1$ (164), $C2/m$ (12), $Cmcm$ (63), and $P2_1/m$ (11), were assumed, in which $Mg^{2+}/Ta^{5+}$ ions are arranged along different directions. Based on the first-principle calculations, the 1:2 ordered BMT with the symmetry $P\bar{3}m1$ (164) is the most stable one. The charge compensation in a cubic phase is obtained only on the average if the B-site ions are distributed randomly, which is called the disordered structure [45], i.e. an effective mean symmetry corresponds to the simple perovskite structure $Pm\bar{3}m(O_h^1)$ space group with $a \simeq a_c$, wherein the A cations are at $(0, 0, 0)$, while both *B′* and *B″* share $(1/2, 1/2, 1/2)$ and oxygen atoms centre the face $(1/2, 1/2, 0)$. However, depending on the nature of the cations, another non-stoichiometric 1:1 ordering exists, which is described as a cubic unit cell ($a \simeq 2a_c$) in the $Fm3m$ space group. The 1:1 ordered model of B cations exist in nanoscale regions, and is called short-range ordering, while the other regions are disordered [46, 47].

The dielectric properties are mainly depended on ionic polarisation and are closely related to lattice dynamics. For example, lattice vibration information is indispensable for understanding dielectric loss, and lattice vibrational spectra of the $A(B'_{1/3}B''_{2/3})O_3$-type MWDCs have been of particular interest [48, 49], i.e. the number and symmetry of the phonon modes can reflect the dielectric properties because the dielectric response at microwave frequencies mainly lie on the characteristics of the polar optical phonons [50]. Therefore, an acquaintance of the phonons is imperative for understanding the dielectric response of MWDCs. Raman scattering and infrared (IR) spectroscopic techniques are extensively applied to study the crystal structures of MWDCs by analysing their optical phonons [51, 52].

Raman scattering spectroscopy is sensitive to ordering–disordering of the local crystal structure. Complex cation arrangements usually lead to changes in the vibrational spectra in comparison with the simple $ABO_3$ structure. Therefore, Raman scattering can play a useful probe to identify the ordering of B-site and evaluate LRO degree of the $A(B'_{1/3}B''_{2/3})O_3$-type MWDCs [53]. It allows spectroscopic evaluation of the degrees of LRO of ordered structures, and one can make use of that information to make a partial assignment of the vibrational modes. Moreover, the study of the Raman spectrum of MWDCs proposed the existence of short-range 1:1 ordered structures [45, 46]. The 1:2 ordered structure-related phonon vibrations have a strong correlation with the microwave properties [50], however, whose intensities are too weak to be detected in many samples. Thus, the characteristics of the oxygen octahedral stretch modes can present the dielectric properties of MWDCs [53]. Also, usually, the ordered structures can be induced by introducing small amounts of tetravalent ions or processing parameters.

The far-IR (FIR) spectroscopic technique can characterise the dielectric response [54], i.e. the FIR spectra of MWDCs respond to the characteristics of lattice vibrations. Ionic radius and 1:2 ordering are important and affect the FIR vibration characteristics. Through a damped oscillator model fitting, such as the classical harmonic oscillator mode, the spectrum can provide the frequencies and damping factors of the phonons, which are related to the crystal structures indirectly and can be used to extrapolate the intrinsic dielectric properties at microwave frequencies. FIR measurements have also been applied to understand the origin of the low-loss MWDCS in terms of the phonon modes [55, 56].

In brief, lattice vibrational spectra, including both Raman and IR spectroscopy, are very useful to study the atomic thermal vibrations of MWDCs, which can provide important information for the crystal structures and the origin of the intrinsic properties. In this review, the lattice dynamics and phonon characteristics of the $A(B'_{1/3}B''_{2/3})O_3$-type MWDCs are presented in detail in order to summarise remarkable progress in this field and make a guide for the design of the next generation advanced MWDCs. The basic theory of the lattice vibration is stated to show its meaning, function, and application to MWDCs, as well as the prediction of the number and type of phonon modes using group theory analysis. The atomic sites and corresponding modes in Raman and FIR spectra are identified, as well as the illustration of the phonon modes are presented for the single phase and solid solution ceramics. The effects of the processing conditions and the ordered superstructures in the nanoscale region on the phonon modes are summarised systemically. The correlations between phonon modes, crystal structures, and dielectric properties are built, which help to create a mathematical model for the structure–property relationships of MWDCs.

## 2 Basic theory about lattice dynamics

### 2.1 Basic concepts of lattice dynamics

The movements of electrons and atomic nucleus dominate the functional properties of most solid materials. By Born–Oppenheimer approximation, the movement of electrons and nuclear can be discussed separately because of the significant differences in mass and velocity between them. The electrons move faster than the nuclear and the movement of the nuclear can be considered as the atomic movement. Lattice dynamics study the vibration of atoms at a finite temperature in crystallised systems, is well developed in the theory of solid-state physics [57–59], which helps to study the macroscopic properties from the microcosmic aspect and is a benefit to creating the correlation of structure–property, also does good to the structure/properties modulation.
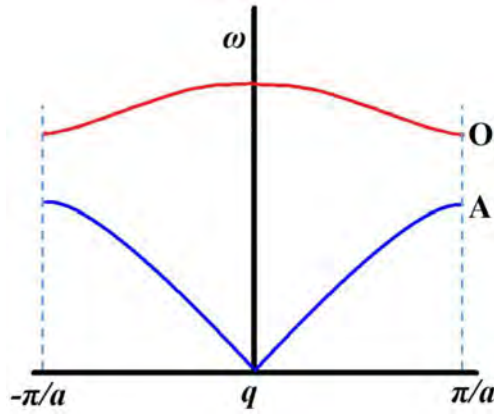
**Fig. 2** *Sketch of phonon dispersion curve in a diatomic chain. A: acoustic branch; O: optical branch*
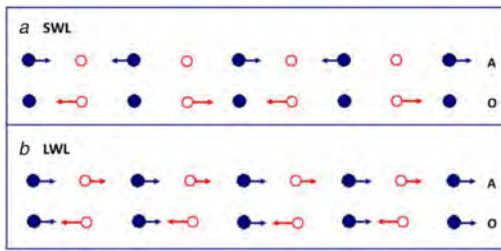


**Fig. 3** *Sketch of lattice wave in a diatomic chain at SWL and LWL. A: acoustic; O: optical*

We take a 1D period diatomic chain as an example to discuss some basic concepts of the lattice dynamics. There are two different independent lattice waves $\omega-$ and $\omega+$, which are defined as acoustic (A) and optical (O) ones, respectively. Plotting the $\omega$–$q$ curve as in Fig. 2, we obtain the dispersion of lattice waves with two branches. $\omega$ is periodic with the periodicity $2\pi/a$, which is the reciprocal lattice constant of the chain. Thus, the lattice waves can be described within the first Brillouin zone from $-\pi/a$ to $+\pi/a$. Furthermore, considering the boundary restriction of the $N$ unit period, only a discrete $q$ is allowed

$$q = 2\pi n/Na. \tag{1}$$

From (2), the displacement pattern (vibrational mode or phonon) is controlled by the wave vector $\boldsymbol{q}$. Thus, there are different vibration patterns and vibration frequencies at different $q$ points. Two limits for these lattice waves are short wavelength limit (SWL, $q\rightarrow\pm\pi/a$) and long wavelength limit (LWL, $q\rightarrow0$, the centre of BZ: $\boldsymbol{\Gamma}$). The vibrational modes of the diatomic chain at these two limits are shown in Fig. 3. Here, we only discussed the longitudinal wave (L), which means that the vibration direction is parallel to wave vector/propagation direction. However, there might be two transverse waves (T) with the vibration perpendicular to the wave vector. The lattice dynamics can also be interpreted by quantum language, where vibrational modes called as phonons have quantised energy ($n$ as an integral number)

$$E = \left(n + \frac{1}{2}\hbar\omega\right). \tag{2}$$

For the 3D crystals, the vibrational modes/phonons and phonon dispersion are very complex. We generally plot the dispersion curve along with some special BZ paths (usually follow the high-symmetry points in the first BZ) and use phonon density of state (integration of the phonon states against vibration frequencies) to describe the phonon properties in the 3D crystals. The phonon dispersion curve often has longitudinal acoustic, transverse acoustic, longitudinal optical (LO) and transverse optical (TO) branches. If there are $N$ atoms in the primitive cell and each atom has three vibration freedoms, $3N$ branches in dispersion curves in the 3D BZ exist. Among these branches, there are three acoustic

ones and $3N-3$ optical ones. There are different vibrational patterns (phonons) with different symmetries at different $\boldsymbol{q}$-points and some phonons might interact with other ones showing multi-phonon (high-order) properties. However, for general vibrational measurements (Raman or IR) discussed here, only the modes at LWL ($\boldsymbol{\Gamma}$ point of BZ) will be detected. Moreover, in most Raman and IR measurements, the high-order phonons show much weaker intensities, which can only be obviously recognised in resonance or high-resolution Raman scattering and high-resolution IR absorption measurements, which are the techniques not popular in current material studies. Thus, we only focus on the first-order $\boldsymbol{\Gamma}$ phonons in this study. These modes have identical vibrations for every primitive cell and reserve all the symmetry operations of the system (crystal symmetry) while modes at other BZ points will lose some symmetries.

## 2.2 Symmetry of vibrational modes

As discussed above, for the vibrational modes in a crystal system, only the primitive unit cell needs to be analysed. These vibrations are constrained by the symmetry of crystallography and can be described using space group theory mathematically. All the equilibrium atomic locations/sites follow specific symmetry operations and each atomic site has its own symmetry. As long as the crystal structure is given, the mode symmetry is determined and can be predicted from group theory analysis. Vibrational modes are displacements of atoms with each Wyckoff site atom correlated by the symmetry. Thus, one can construct the components from group theory analysis using atomic displacement (vector) as freedoms. These component displacements are called symmetry coordinates of vibrational modes showing special symmetry (e.g. $A_g$, $A_u$, $E$) and basis (e.g. translatory $T_x$, $T_y$, $T_z$, rotary $R_x$, $R_y$, $R_z$, polarisability $\alpha_{xx}$, $\alpha_{xy}$ etc) [60]. Symmetry coordinate symbols are often marked as small letters (e.g. $a_g$, $a_u$) to be distinguished from phonon modes symbols. The exact vibrational modes are linearly combined symmetry coordinates with the same symmetry. For example, there are four $a_g$ symmetry coordinates in Mg–Ta ordered BMT and four $A_g$ vibrational models are combined [48]. Generally, the exact proportions of symmetry coordinates in a vibrational mode can only be decided from the Hessian matrix, which means the atomic mass and force field are needed. There are many different ways to calculate the vibrational modes of single crystals, of which, density functional theory calculation is a very successful method [61–63].

For lattice dynamics, the most important thing is to study the thermal movement of atoms, especially their reflection in Raman and FIR spectroscopies. The modes should be assigned and illustrated accurately, i.e. people can know what atom and which movement cause these vibrations, and also know the relationship between lattice vibrations and structures or properties

$$P = \alpha E = \alpha_0 E\cos(\omega_1 t - \boldsymbol{k}_1 \cdot \boldsymbol{r})$$
$$+ \frac{1}{2}\Delta\alpha_0 E\{\cos[(\omega_1 - \omega)t - (\boldsymbol{q} - \boldsymbol{k}_1)\cdot\boldsymbol{r}] \tag{3}$$
$$+ \cos[(\omega_1 + \omega)t - (\boldsymbol{q} + \boldsymbol{k}_1)\cdot\boldsymbol{r}]\},$$

where $\alpha$ is the polarisability tensor, which is the equilibrium electronic polarisability $\alpha_0$ coupled with Raman active vibration polarisability $\Delta\alpha_0$. $\omega_1$ is the angular frequency, $\boldsymbol{k}_1$ is a wave vector of incident photons; $\omega$ is angular frequency, $\boldsymbol{q}$ is a wave vector of Raman modes. The three items in the formula are Rayleigh scattering (elastic), Stokes Raman scattering ($\omega_1 - \omega$) and anti-Stokes Raman scattering ($\omega_1 + \omega$). Raman intensity is determined by the Raman tensor and influenced by the measurement geometry, which means the relations between the polarisation direction of incident/scattered light and crystal axis [64]. The Raman measurement geometry can be written as Porto's notation $k(mn)l$, where $k$ is the direction of the propagation of incident light, $l$ is the scattered light; $m$ is the direction of the polarisation of incident light and $n$ is the scattered light [65, 66], e.g. $x(yz)\bar{x}$ means the back scattering Raman measurement with excited light coming from $x$

and scattered light returning along the $-x$-axis and the polarisation planes of incident and scattered light are parallel to the $y$- and $z$-axis.

## 2.3 Raman spectra of solid-state materials

Raman scattering is an inelastic scattering of incident photons from the phonons in materials. Raman spectroscopy makes use of monochromatic light to excite its inelastic scattering in the crystal lattice. The vibrational modes belong to a given crystal structure which underpins the origin of the individual Raman bands. As the vibrational modes themselves, the Raman bands are intimately related to the crystallographic structure details, such as texture, orientation, and lattice distortions (e.g. those arising from the effect of an applied and/or residual stress state).

Regarding the information of Raman modes, two parameters should be noticed: (i) the relative intensity of different Raman bands is related to both the structure and orientation of the crystal through the so-called 'Raman selection rules' and (ii) the apical shift of Raman bands representing individual vibrational modes in a certain crystal is related to the stress tensor stored in the probed region through a (structure-dependent) secular equation, in which a set of constants (i.e. the phonon deformation potential) describes the stiffness of crystal lattice vibrations with respect to a standard (relaxed) condition [67].

Raman technology is one of the useful tools to study the crystal structures of MWDCs. Using group theory analysis, the assignment and illustration of the vibrations of an $A$–$B'$–$B''$–$O$ system by the normal modes can be established [45, 52].

## 2.4 FIR spectra of solid-state materials

The refractive index $n$ ($n = \varepsilon^{1/2}$) and the extinction coefficient $\kappa$ are commonly used basic parameters, which can describe the optical properties of a material. These two parameters are closely related to the complex dielectric constant $\varepsilon^*(\omega) = \varepsilon'(\omega) + i\varepsilon''(\omega)$. Reflectivity ($R$) is an important parameter (a fitting function of the original date) of the IR reflection spectra, which refers to the ratio of the reflected light intensity and the incident light intensity when light irradiates vertically from vacuum to the material surface. $F$ is the fitting function after the analytical continuation

$$n = \frac{1 - (R/100)}{(R/100) - (2*\sqrt{R/100})*\cos[F] + 1}, \tag{4}$$

$$k = \frac{(2*\sqrt{R/100})*\sin[F]}{(R/100) - (2*\sqrt{R/100})*\cos[F] + 1}. \tag{5}$$

When atoms in the molecule absorb energy and energy level transition occurs, rotational energy level transition will occur inevitably, and thus, the vibration–rotation spectrum can be called the IR reflection spectrum. Based on the dispersion theory, complex permittivity, $\varepsilon'$ and $\varepsilon''$, can be described by the following equations:

$$\varepsilon' = n^2 - k^2, \quad \varepsilon'' = 2nk. \tag{6}$$

Most of the vibrational modes in solid systems are $<1500\ \mathrm{cm}^{-1}$, which are located in the mid-IR and FIR regions. A polar vibration in 3D space shows different frequencies along different propagations (TO versus LO) because restoring force for LO is enhanced by the polarisation extra electric field, therefore, increases the frequency. This is called LO–TO splitting of polar modes, which obeys Lyddane–Sachs–Teller relation [35]

$$\frac{\omega_{\mathrm{LO}}^2}{\omega_{\mathrm{LO}}^2} = \frac{\varepsilon_{\mathrm{s}}}{\varepsilon_{\infty}}, \tag{7}$$

where $\omega_{\mathrm{TO}}$ and $\omega_{\mathrm{LO}}$ are the frequencies of TO and LO modes, $\varepsilon_{\mathrm{s}}$ and $\varepsilon_{\infty}$ are the static and optical frequency dielectric constant. There are two typical methods to measure the FIR modes: absorption/transmission or reflection. For the FIR absorption measurement,

the TO frequencies of FIR modes will be detected. However, most solid materials have very strong IR absorption and it is quite difficult to acquire a high-quality FIR absorption spectrum. Thus, the FIR reflection spectra are more popular than absorption ones. In FIR reflection spectra, an FIR mode can be considered as a damped oscillator and the spectra can be fitted by either Lorentz three-parameter classical model [(8)] [68] or four-parameter semi-quantum model (FPSQ) [(9)] [55, 69]

$$\varepsilon^*(\omega) = \varepsilon_{\infty} + \sum_{j=1}^{n} \frac{\omega_{j\mathrm{TO}}^2 S_{j\mathrm{TO}}}{\omega_{j\mathrm{TO}}^2 - \omega^2 + i\omega\gamma_{j\mathrm{TO}}}, \tag{8}$$

$$\varepsilon^*(\omega) = \varepsilon_{\infty} \prod_{j=1}^{n} \frac{\omega_{j\mathrm{LO}}^2 - \omega^2 + i\omega\gamma_{j\mathrm{LO}}}{\omega_{j\mathrm{TO}}^2 - \omega^2 + i\omega\gamma_{j\mathrm{TO}}}, \tag{9}$$

where $\varepsilon_{\infty}$ is the optical frequency permittivity caused by electropolarisation; $n$ is the FIR mode number; $\omega_{j\mathrm{TO}}$, $\omega_{j\mathrm{LO}}$, and $\gamma_{j\mathrm{TO}}$, $\gamma_{j\mathrm{LO}}$ are frequencies and damping factors of the $j$th TO mode and the $j$th LO mode, $S_{j\mathrm{TO}}$ is $j$th TO mode strength.

FIR reflectivity ($R$) can be represented by Fresnel equation expressed below, i.e. $R$, $\varepsilon(\omega)$, $n$, and $\kappa$ are interrelated, which shows the relationship between the IR spectra and the complex permittivity

$$R = \left| \frac{\sqrt{\varepsilon(\omega) - 1}}{\sqrt{\varepsilon(\omega) + 1}} \right|^2 = \frac{(n-1)^2 + k^2}{(n+1)^2 + k^2}. \tag{10}$$

## 2.5 Group theory analysis and selection rules

As the vibrational modes are a linear combination of symmetry coordinates with the same symmetry class, the number and optical activity (Raman or IR selection rules) of vibrational modes can be obtained immediately from the group theory analysis of the symmetry coordinates. Vibrational modes with different symmetries may have different optical activities. The first-order optical active modes are much more intensive than higher ones. Thus, we only discuss the first-order activity here. A mode is IR active if the vibration changes dipole moment and it is Raman active if it changes polarisability tensor. These can be described by different basis functions in character tables. The IR active ones have a translatory basis ($T_x$, $T_y$, $T_z$ or $x$, $y$, $z$) whilst Raman active ones have porlarisability or quadratic basis ($\alpha_{xx}$, $\alpha_{xy}$, $x^2$ etc.). It should be mentioned again that in all crystal systems, there are three acoustic modes, which means all the atoms vibrate as a whole either along $x$, $y$ or $z$ directions. Acoustic modes do have the same basis with the IR modes but are not IR active ones.

Two different approaches can be applied to explain the lattice vibrational spectra of MWDCs [14, 27]. The first method indicates that the disorder in B-sites contributes to the first-order Raman scattering characteristics, which are concerned with translational and inversion symmetries losses. The second method suggests the ordered regions with special symmetry, which allows the occurrence of extra Raman modes not permitted for cubic structures. Both approaches are useful in real ceramics because these two methods are not mutually exclusive. Reviewing the previous study on vibrational spectra of the $A(B'_{1/3}B''_{2/3})O_3$-type complex perovskite MWDCs, one can note three possible contribution factors which contribute to the appearance of the Raman spectra: the relaxation of the selection rules, the 1:1 ordering and B site with 1:2 ordering [27].

B sublattice in $A(B'_{1/3}B''_{2/3})O_3$-type MWDCs is made up of the ions with different valence states in a 1:2 ratio. An effective mean symmetry corresponding to the simple cubic perovskite structure appears when the B-site ions are a random distribution. However, the ideal cubic perovskite structure is not Raman-active in the first-order vibrational spectrum [46, 70]:

$$\Gamma_{\mathrm{V}} = 3F_{1u}(IR) + F_{2u}(-) + F_{1u}(A), \tag{11}$$

where IR denotes IR activity, $A$ denotes acoustic mode, and $F_{2u}(-)$ mode is silent (non-active) in the spectra, respectively. Considering the predominant role of disordering, the Raman-active modes were related to the loss of both translational and inverse symmetries to disordering in the B-sites. The selection rules for Raman scattering relaxed in such a system, so light scattering becomes possible from some points in the Brillouin zone.

The second possibility also existed for the occurrence of the Raman modes was confirmed in the most recent publications. The B-site with 1:1 ordering exists in nano-regions. The ceramic with a 1:1 superstructure presents the cubic symmetry, for which the group theory analysis yields the following modes:

$$\Gamma_V = A_{1g}(R) + E_g(R) + 2F_{2g}(R)$$
$$+ 4F_{1u}(IR) + F_{1g}(-) + F_{2u}(-), \quad (12)$$

where $R$ is the Raman mode, IR is the IR active mode, and $-$ denotes silent (non-active) mode, respectively. Four Raman active modes are allowed in the cubic $Fm3m$ symmetry. The $B^{2+}$ and $B^{5+}$ 1:2 ordered arrangements lead to the trigonal structure, with ($P\bar{3}m1$) space group with the symmetries and mode numbers as follows [46]:

$$\Gamma_V = 4A_{1g}(R) + 5E_g(R) + 7A_{2u}(IR)$$
$$+ 9E_u(IR) + A_{2g}(-) + A_{1u}(-). \quad (13)$$

There are nine Raman active modes, i.e. $4A_{1g} + 5E_g$, which have a relationship with the motion of $A$ and $B''$ ions at the $2d$ sites, and the motion of $O^{2-}$ caption at the $6i$ sites [71–73].

The 1:2 ordered structure of $A(B'_{1/3}B''_{2/3})O_3$-type complex perovskite MWDCs belong to the ($P\bar{3}m1$) space group. 15 atoms exist in the primitive cell with 45 degrees of freedom, whose Wyckoff sites are distributed as follows: two A ions occupy $2d$ sites and one $A$ ion occupies a $1b$ site ($1a$ site, in [48]); the two $B''$ ions are on $2d$ sites; one $B'$ ion is on a $1a$ site ($1b$ site, in [74]); six O ions are on $6i$ sites; and three O ions are on $3f$ sites ($3e$ sites, in [74]). The distribution of the vibrational modes of the 1:2 ordered structures in terms of the irreducible representations of the $D_{3d}$ factor-group at $\Gamma$-point of the first Brillouin zone is $A_{2u} + E_u$ (acoustic), $A_{2g} + 2E_{2u}$ (silent), $7A_{2u} + 9E_u$ (IR), and $4A_{1g} + 5E_g$ (Raman) [49]. Therefore, up to nine Raman-active modes and 16 IR-active modes can be expected for the 1:2 ordered $A(B'_{1/3}B''_{2/3})O_3$-type complex perovskite ceramic [28].

In general, each vibrational mode (Raman or FIR mode) can be attributed to the movements of all of the atoms. However, given the symmetric restriction in MWDCs, the atoms at the sites of Ba ($1a$ or $1b$), Mg/Zn ($1b$ or $1a$) and O ($3e$) are not involved in the Raman vibrations, and only the atoms Ba ($2d$ site), Ta/Nb ($2d$ site), and O ($6i$ site) have contribution to Raman active modes according to group theory analysis. Based on the symmetric restrictions, each atom presents some special vibration patterns, i.e. symmetry coordinates [60, 75]. All vibrational modes are the combination of the symmetry coordinates in the same point group [48, 76]. The symmetry coordinates identify with the vibrational modes in systems with strong covalence bonds.

## 3 Raman phonon mode characteristics of MWDCs

### 3.1 Assignment and illustration of Raman phonon modes

Raman spectra are highly sensitive to the composition and crystal structure. Raman shifts (frequencies), intensities, and the full width at half maximum (FWHM) values in Raman modes of MWDCs, caused by substitution of atoms in $A$-, $B'$-, $B''$- sites and additives, are important features in distinguishing the normal modes, i.e. the change of the spectral profile caused by different compositions is meaningful to assign and illuminate Raman modes for every concrete MWDC. Raman modes of the representative single-phase MWDC ceramics such as BMT, Ba(Mg$_{1/3}$Nb$_{2/3}$)O$_3$ (BMN), Ba(Zn$_{1/3}$Ta$_{2/3}$)O$_3$ (BZT) and Ba(Mg$_{1/3}$Zn$_{2/3}$)O$_3$ (BZN), were previously studied by several researchers [43, 45, 48, 73, 76], as shown in Table 1.

Take BMN as an example. The vibration occurs at the $\Gamma$ point of the first Brillouin zone, and the ions move similarly and the displacements have 45 coordinates [27], which imply irreducible representations, i.e. normal modes.

The Billbao Crystallographic Center website [64] provides information about the optical modes of BMN, which can be represented as follows:

$$\Gamma_V = 4A_{1g}(R) + 5E_g(R) + 7A_{2u}(IR)$$
$$+ 9E_u(IR) + A_{2g}(-) + 2A_{1u}(-). \quad (14)$$

From the above formula, BMN has nine Raman-active modes ($4A_{1g}$, $5E_g$), 16 IR-active modes ($7A_{2u}$, $9E_u$), and three silence modes ($A_{2g}$, $2A_{1u}$). In short, the ordered BMN ceramic presents

**Table 1** The concrete sites, assignment, and description of single-phase MWDCs

| BMT [48] | | Site symmetry | Vibration type or description | BMT [77] | | Site symmetry | Vibration type or description |
|---|---|---|---|---|---|---|---|
| $E_g$(Ba) | 104 cm$^{-1}$ | $2d$ | twisting vibration of Ba–TaO$_6$ on the $ab$ plane | $F_g$(Ba) = $A_{1g}$(Ba) + $E_g$(Ba) | 105 cm$^{-1}$ | $2d$ | two overlapping bands, the modes in the intermediate frequency range can be attributed to the internal vibrations of Ta in TaO$_6$ octahedra |
| $A_{1g}$(Ba) | 107 cm$^{-1}$ | | stretching vibration of Ba–TaO$_6$ along $c$-axis | $E_g$(O) | 171 cm$^{-1}$ | $6i$ | the 1:2 ordered structure-related vibrations |
| $A_{1g}$(Ta) | 212 cm$^{-1}$ | $2d$ | breath-vibration along $c$-axis | $E_g$(Nb) | 263 cm$^{-1}$ | $2d$ | |
| $E_g$(Ta) | 160 cm$^{-1}$ | | twisting vibrations of O$_3$–Ta–O$_3$ on the $ab$ plane | $A_{1g}$(Nb) | 296 cm$^{-1}$ | | |
| $E_g$(Ta) | 264 cm$^{-1}$ | | twisting breath-vibration of O ($6i$ site) octahedra along $c$-axis | $F_g$(O) = $A_{1g}$(O) + $E_g$(O) | 386 cm$^{-1}$ | $6i$ | Moreira et al. [51] think there are nine Raman modes for ordered ceramics and five additional bands due to disorder or defect [27] |
| $E_g$(O) | 386 cm$^{-1}$ | $6i$ | twisting breath-vibrations | $E_g$(O) | 437 cm$^{-1}$ | | |
| $A_{1g}$(O) | 433 cm$^{-1}$ | | breath-vibration along $c$-axis and in $ab$-plane is expanding and shrinking at the same time | $A_{1g}$(O) | 788 cm$^{-1}$ | | breathing of the oxygen octahedra |
| $E_g$(O) | 576 cm$^{-1}$ | | twisting breath-vibrations | — | — | — | — |
| $A_{1g}$(O) | 798 cm$^{-1}$ | | breath-vibration along $c$-axis is expanding and breath-vibration in $ab$-plane is shrinking | — | — | — | — |

| BZT [71] | Site symmetry | Vibration type or description | BZT [78] | | Site symmetry | Vibration type or description |
|---|---|---|---|---|---|---|
| $A_{1g}$(Ba) 106 cm$^{-1}$ | 2d | phonons related to the Ba atomic motion | $F_g$(Ba) = $A_{1g}$(Ba) + $E_g$(Ba) | 104.6 cm$^{-1}$116.7 cm$^{-1}$ | 2d | two overlapping bands |
| $E_g$(O)  157 cm$^{-1}$ | 6i | 1:2 ordered phonons | $E_g$(O) | 154.6 cm$^{-1}$ | 6i | 1:2 ordered phonons |
| $E_g$(Ta)  212 cm$^{-1}$ | 2d | | $E_g$(Ta) | 209.7 cm$^{-1}$ | 2d | |
| $A_{1g}$(Ta) 260 cm$^{-1}$ | | | $A_{1g}$(Ta) | 261.7 cm$^{-1}$ | | |
| $F_{2g}$(O) 376 cm$^{-1}$ | 6i | modes related to the O atomic motion | $F_{2g}$(O) | 373.2 cm$^{-1}$ | 6i | modes related to the O atomic motion |
| $E_g$(O)  427 cm$^{-1}$ | | | $E_g$(O) | 423.2 cm$^{-1}$ | | |
| $A_{1g}$(O) 811 cm$^{-1}$ | | oxygen-octahedron stretch modes | $A_{1g}$(O) | 800.3 cm$^{-1}$ | | oxygen-octahedron stretch modes |

| BMN [73] | Site symmetry | Vibration type or description | BMN [43] | Site symmetry | Vibration type or description |
|---|---|---|---|---|---|
| $A_{1g}$ + $E_g$ 105 cm$^{-1}$ | 2d | Ba vibrational mode | $F_{2g}$(Ba)  106 cm$^{-1}$ | 2d | phonons related to the Ba atomic motion near 105 cm$^{-1}$ |
| $E_g$(O)  175 cm$^{-1}$ | 6i | 1:2 ordered phonons | $E_g$(O)  175.4 cm$^{-1}$ | 6i | 1:2 ordered structure-related vibrations |
| $E_g$(Nb)  263 cm$^{-1}$ | 2d | | $E_g$(Nb)  264.1 cm$^{-1}$ | 2d | |
| $A_{1g}$(Nb) 296 cm$^{-1}$ | | | $A_{1g}$(Nb) 296.9 cm$^{-1}$ | | |
| $F_{2g}$(O)  386 cm$^{-1}$ | 6i | O vibrational modes | $F_{2g}$(O)  386.6 cm$^{-1}$ | 6i | modes related to the O atomic motion in between 350 and 450 cm$^{-1}$ |
| $E_g$(O)  437 cm$^{-1}$ | | | $E_g$(O)  435.8 cm$^{-1}$ | | |
| $A_{1g}$(O)  788 cm$^{-1}$ | | oxygen-octahedron stretch modes | $A_{1g}$(O) 788.7 cm$^{-1}$ | | oxygen-octahedron stretch modes |

| BZN [78] | Site symmetry | Vibration type or description | BZN [43] | Site symmetry | Vibration type or description |
|---|---|---|---|---|---|
| — | — | — | $F_{2g}$(Ba)  106 cm$^{-1}$ | 2d | phonons related to the Ba atomic motion near 105 cm$^{-1}$ |
| $E_g$(O)  174 cm$^{-1}$ | 6i | 1:2 ordered phonons | $E_g$(O)  171.6 cm$^{-1}$ | 6i | 1:2 ordered structure-related vibrations |
| $E_g$(Nb)  269 cm$^{-1}$ | 2d | | $E_g$(Nb)  — | | |
| $A_{1g}$(Nb) 294 cm$^{-1}$ | | | $A_{1g}$(Nb) 304.6 cm$^{-1}$ | 2d | |
| $F_{2g}$(O)  378 cm$^{-1}$ | 6i | O vibrational modes | $F_{2g}$(O)  372 cm$^{-1}$ | 6i | modes related to the O atomic motion in between 350 and 450 cm$^{-1}$ |
| $E_g$(O)  429 cm$^{-1}$ | | | $E_g$(O)  437.7 cm$^{-1}$ | | |
| $A_{1g}$(O) 782 cm$^{-1}$ | | oxygen-octahedron stretch modes | $A_{1g}$(O) 784.8 cm$^{-1}$ | | oxygen-octahedron stretch modes |
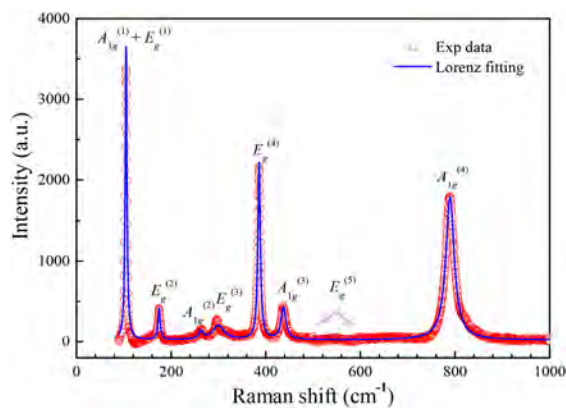


**Fig. 4** *Raman spectra of BMN [73]*

nine Raman active modes, while the disordered material has 11 predicted modes, as shown in Fig. 4. Given the symmetric restriction, the atoms at the sites of Ba(1a), Mg(1b) and O(3e) are not involved in the Raman vibrations. The low-frequency modes $A_{1g}^{(1)}$ (105 cm$^{-1}$) and $E_g^{(1)}$ (105 cm$^{-1}$) belong to external vibration of Ba against NbO$_6$ octahedron. The $A_{1g}^{(1)}$ mode is the stretching vibration of NbO$_6$ along the $c$-direction, whereas the $E_g^{(1)}$ mode is the twisting vibration of Ba–NbO$_6$ on the $ab$-plane. The modes in the intermediate frequency range are the internal vibrations of Nb in NbO$_6$ octahedron. The $A_{1g}^{(2)}$ and $A_{1g}^{(3)}$ modes are the different stretching vibrations of O$_3$–Nb–O$_3$ along the $c$-direction, whereas the $E_g^{(2)}$, $E_g^{(3)}$, $E_g^{(4)}$, and $E_g^{(5)}$ modes belong to the twisting vibrations of O$_3$–Nb–O$_3$ on the $ab$-plane. $A_{1g}^{(4)}$ with the highest frequency (789 cm$^{-1}$) is also an internal mode.

The Raman mode assignment for BMN was also conducted by Moreira *et al.* [51], Payne *et al.* [79] and Liu *et al.* [80]. Generally speaking, four main Raman modes are related to the vibrations of the 1:1 ordered structure and other modes are the vibrations of the 1:2 ordered structure. The vibrations modes of localised 1:1 ordered and long-range 1:2 ordered structures are made up of four feature regions: (i) the Raman mode near 105 cm$^{-1}$ is associated with $F_{2g}$(Ba) of the 1:1 ordered structure; (ii) two modes near 400 cm$^{-1}$ correspond to the vibration of O atoms; (iii) the $A_{1g}$(O) mode near 800 cm$^{-1}$ is the oxygen octahedron stretch mode, which relates to the 1:1 ordered structure; (iv) three weak phonons

between 150 and 350 cm$^{-1}$ are identified as the 1:2 ordered structure-related vibrations. The $F_{2g}$(O) at about 386 cm$^{-1}$ was assigned to $A_{1g}$(O) + $E_g$(O). [73]. The weak peak $E_g$(5) at 576 cm$^{-1}$ can be assigned to $E_g$(O,6i) as reported in Wang's [47] work. In brief, only atoms at the sites of Ba(2d), Nb/Ta(2d), and O(6i) contribute to the Raman modes, and heavy cations give many contributions to the low-frequency vibration modes; in contrast, the light ones, i.e. O contributes to the high-frequency modes.

Ion substitution can change the symmetry and the ordered degree of $A(B'_{1/3}B''_{2/3})O_3$-type MWDCs, which can be proved by the new Raman modes, Raman shifts or the splitting of Raman modes etc. The concrete sites, assignment and description of the MWDCs

with A- and B-site substitution are concluded and shown in Table 2.

Take the $(Ba_{1-x}Sr_x)(Zn_{1/3}Nb_{2/3})O_3$ (BSZN) solid solutions as an example. Raman mode assignments for the BSZN were conducted in our previous work. The results showed that two weak modes appear near the range of 150–300 cm$^{-1}$ (0 < $x$ ≤ 0.6), similar to the results of [77, 85], and three extra modes appear in the samples where $x$ ≥ 0.65, indicating a change in the crystal structures, i.e. gradually varying from cubic ($Pm\bar{3}m$) symmetry to pseudo-cubic ($I4/mcm$) phase and finally to hexagonal symmetry.

In brief, ion substitution changes the symmetry and ordered degree, which leads to the appearance of the new Raman mode, a variation of FWHM values, the mode splitting or frequency shifts.

**Table 2** Concrete sites, assignment, and description of MWDCs with ions substitution

| $(Ba_{0.7}Sr_{0.3})$ $(Mg_{1/3}Nb_{2/3})O_3$ | BSMN [81] | Site symmetry | Vibration type or description | $(Ba_{0.7}Sr_{0.3})$ $(Zn_{1/3}Nb_{2/3})O_3$ | BSZN [52] | Site symmetry | Vibration type or description |
|---|---|---|---|---|---|---|---|
| $A_{1g} + E_g$ | 94.6 cm$^{-1}$119 cm$^{-1}$ | 2d | lattice vibrations of Ba and Sr ions | $F_{2g}$(Ba) | 104.4 cm$^{-1}$ | 2d | Ba and Sr vibrational modes associated with the 1:1 ordered structure |
| $E_g$(O) | 174 cm$^{-1}$ | 6i | modes associated with oxygen ions | $E_g$(O) | 185.1 cm$^{-1}$ | 6i | phonons related to the 1:2 ordered structure |
| $E_g$(Nb) | 263 cm$^{-1}$ | 2d | bands due to niobium ions | $E_g$(Nb) | 230 cm$^{-1}$ | 2d | |
| $A_{1g}$(Nb) | 296 cm$^{-1}$ | | | $A_{1g}$(Nb) | 292.9 cm$^{-1}$ | | |
| $E_g$(O) | 386 cm$^{-1}$ | 6i | modes associated with oxygen ions | $F_{2g}$(O) | 379 cm$^{-1}$ | 6i | phonons associated with the 1:1 ordered structure |
| $E_g$(O) | 437 cm$^{-1}$ | | | $E_g$(O) | 432.5 cm$^{-1}$ | | |
| $A_{1g}$(O) | 788 cm$^{-1}$ | | | $A_{1g}$(O) | 819.3 cm$^{-1}$ | | oxygen-octahedron stretch modes |
| — | 136.3 cm$^{-1}$, 237.6 cm$^{-1}$, 423.4 cm$^{-1}$,… | — | extra bands due to tilting of oxygen octahedra | — | — | — | — |

| $Ba[(Zn_{0.4}Mg_{0.6})_{1/3}Nb_{2/3}]O_3$ | BZMN [43] | Site symmetry | Vibration type or description | $Ba[(Zn_{0.4}Mg_{0.6})_{1/3}Ta_{2/3}]O_3$ | $Ba[(Zn_{0.4}Mg_{0.6})_{1/3}Ta_{2/3}]O_3$ [82] | Site symmetry | Vibration type or description |
|---|---|---|---|---|---|---|---|
| $F_{2g}$(Ba) | 106 cm$^{-1}$ | 2d | Ba vibration mode associated with a 1:1 ordered structure | $F_{2g}$(Ba) | 103.6 cm$^{-1}$, 106.6 cm$^{-1}$ | 2d | phonons related to the Ba atomic motion near 105 cm$^{-1}$. |
| $E_g$(O) | 173.5 cm$^{-1}$ | 6i | 1:2 ordered phonons | $E_g$(O) | 156 cm$^{-1}$ | 6i | 1:2 ordered structure-related vibrations |
| $E_g$(Nb) | 264.1 cm$^{-1}$ | 2d | — | $E_g$(Nb) | 210 cm$^{-1}$ | 2d | — |
| $A_{1g}$(Nb) | 296.9 cm$^{-1}$ | — | — | $A_{1g}$(Nb) | 296.9 cm$^{-1}$ | — | — |
| $E_g$(O) | 383.7 cm$^{-1}$ | 6i | O vibration modes | $F_{2g}$(O) | 386.6 cm$^{-1}$ | 6i | modes related to the O atomic motion in between 350 and 450 cm$^{-1}$ |
| $E_g$(O) | 434 cm$^{-1}$ | — | — | $E_g$(O) | 435.8 cm$^{-1}$ | — | — |
| $A_{1g}$(O) | 790.6 cm$^{-1}$ | — | oxygen-octahedron stretch modes | $A_{1g}$(O) | 788.7 cm$^{-1}$ | — | oxygen-octahedron stretch modes |

| $x$Ba(Mg$_{1/3}$Ta$_{2/3}$)O$_3$–(1 − $x$)Ba(Mg$_{1/3}$Nb$_{2/3}$)O$_3$ | $x$BMT–(1 − $x$)BMN [72] | Site symmetry | Vibration type or description | Ba[Zn$_{1/3}$(Nb$_{0.4}$Ta$_{0.6}$)$_{2/3}$]O$_3$ | BZNT [78] | Site symmetry | Vibration type or description |
|---|---|---|---|---|---|---|---|
| $A_{1g} + E_g$ | 105 cm$^{-1}$ | 2$d$ | Ba vibrational mode | $F_{2g}$(Ba) | 106 cm$^{-1}$ | 2$d$ | phonons related to the Ba atomic motion near 105 cm$^{-1}$ |
| $E_g$(O) | 158–175 | 6$i$ | 1:2 ordered phonons | $E_g$(O) | 175.4 cm$^{-1}$ | 6$i$ | 1:2 ordered structure-related vibrations |
| $E_g$(Nb/Ta) | 211–263 | 2$d$ | — | $E_g$(Nb/Ta) | 264.1 cm$^{-1}$ | 2$d$ | — |
| $A_{1g}$(Nb/Ta) | 264–296 | — | — | $A_{1g}$(Nb/Ta) | 296.9 cm$^{-1}$ | — | — |
| $E_g$(6O) | 386 cm$^{-1}$ | 6$i$ | O vibrational modes | $F_{2g}$(O) | 386.6 cm$^{-1}$ | 6$i$ | modes related to the O atomic motion in between 350 and 450 cm$^{-1}$ |
| $E_g$(6O) | 437 cm$^{-1}$ | — | — | $E_g$(O) | 435.8 cm$^{-1}$ | — | — |
| $A_{1g}$(6O) | 788–797 | — | oxygen–octahedron stretch modes | $A_{1g}$(O) | 788.7 cm$^{-1}$ | — | oxygen–octahedron stretch modes |

| Ba[Mg$_{0.8/3}$Zr$_{0.2}$Ta$_{1.6/3}$]O$_3$ | BMZrT [83] | Site symmetry | Vibration type or description | Ba[M$_{g0.3}$Zr$_{0.1}$Nb$_{0.6}$]O$_3$ | BMZrN [84] | Site symmetry | Vibration type or description |
|---|---|---|---|---|---|---|---|
| $F_{2g}$(Ba)=$A_{1g} + E_g$ | 106 cm$^{-1}$ | 2$d$ | Ba vibrational mode | $F_{2g}$(Ba) | 108 cm$^{-1}$ | 2$d$ | phonons related to the Ba atomic motion near 105 cm$^{-1}$ |
| $E_g$(O) | 175 cm$^{-1}$ | 6$i$ | The 1:2 ordered phonons | $E_g$(O) | 172 cm$^{-1}$ | 6$i$ | The 1:2 ordered structure-related vibrations |
| $A_{1g}$(Nb) | 296 cm$^{-1}$ | 2$d$ | | $A_{1g}$(Nb) | 304 cm$^{-1}$ | 2$d$ | — |
| $F_{2g}$(O) = $A_{1g}$(O) + $E_g$(O) | 376 cm$^{-1}$ | 6$i$ | O vibrational modes | $F_{2g}$(O) | 410 cm$^{-1}$ | 6$i$ | modes related to the O atomic motion in between 350 and 450 cm$^{-1}$ |
| $E_g$(O) | 429 cm$^{-1}$ | — | — | $E_g$(O) | 445 cm$^{-1}$ | — | — |
| $A_{1g}$(O) | 788 cm$^{-1}$ | — | oxygen-octahedron stretch modes | $A_{1g}$(O) | 774 cm$^{-1}$ | — | oxygen-octahedron stretch modes |

In all likelihood, the reason for the new modes is due to the effect of the crystal lattice distortion, sometimes maybe due to antiphase oxygen octahedral distortion. The higher-ordered degree, the stronger intensity of Raman peaks. The phonon mode activities lie on the local or long-range symmetry.

### 3.2 Effect of ordered/disordered superstructures on Raman phonon modes

Nagai *et al.* [37] developed new models to explore the 1:2 ordered structures and the oxygen octahedral distortion of $A(B'_{1/3}B''_{2/3})O_3$-type MWDCs, and thought the structural change of BSMT ceramics is related to the strontium substitution. Subsequently, the BSMN ceramics are $P\bar{3}m1$ researched and two regions: the 1:2 ordered trigonal structures and the 1:2 chemical ordered structures are identified by Lee *et al.* [86], without and with the tilting of the oxygen octahedron, respectively.

Particularly, $A(B'_{1/3}B''_{2/3})O_3$-type MWDCs have shown the lowest loss value, i.e. the high $Q \times f$ value, which is related to the cationic order–disorder in B-sites. The LRO of $B'/B''$ at B-sites affects the $Q \times f_0$ of MWDCs, i.e. tan $\delta$ decreases drastically with increasing LRO degree of B-site ions, and the ceramics with highly ordered $B'/B''$ ions at B-sites show large $Q \times f_0$ factors, i.e. low-dielectric losses. Raman spectroscopy is used to probe the 1:2 ordered structures in $A(B'_{1/3}B''_{2/3})O_3$-type ceramics [87, 88], which offers the possibility of detecting a small-ordered region. As the B-site ions have a random distribution, the MWDC structure is usually disordered cubic perovskite. While in the ordered ceramics, a stacking sequence is made up of these cations.

As discussed above, the Raman spectrum is sensitive to the change of ordered structures. Typical Raman spectra of the $A(B'_{1/3}B''_{2/3})O_3$-type complex perovskite ceramics with the 1:2 ordered structure, e.g. BZT, BMT, and BMN, have four main peaks related to the localised 1:1 ordered structure. Three weak phones at 150 and 300 cm$^{-1}$ are highly correlated with the long-range 1:2 ordered structures [89, 90], and the localised 1:1 ordered $F_{2g}$ mode splits into $A_{1g}$ and $E_g$ modes with the long-range 1:2 order preserved [72].

Wang [47] pointed out that the ceramics with higher-ordered degree exhibits sharp Raman peaks, while the samples with lower-ordered degree show shouldered peaks. When the ordered degree increases, the local symmetry changes, and thus some Raman inactive modes may be activated. In short, with the increase in the ordered degree, the peak becomes sharper, i.e. the width becomes narrower, which corresponds to the Moreira's conclusion [51].
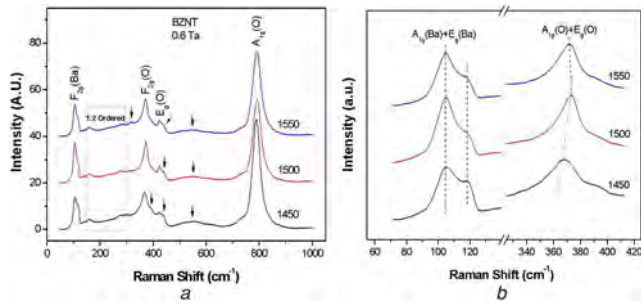
**Fig. 5** *Raman spectra of BZNT ceramics with different Ts*
*(a)* Raman spectra of BZNT at different Ts, *(b)* $F_{2g}$(Ba) and $F_{2g}$(O) modes of the BZNT [92]

### 3.3 Effect of processing conditions on Raman modes of MWDCs

The ordered structures depend on the processing conditions greatly [91], and B-site ordering is obviously influenced by sintering temperature (Ts) and sintering time. The ordered degree can be improved by annealing [92] and results in the increasing Q factor, i.e. the composition, Ts, and sintering time (or soaking time) can affect the ordered structures, which can be reflected in the Raman spectra.

In general, with increasing of Ts, the Raman peaks of the MWDCs show a slight shift towards higher frequencies and become narrower (small FWHW values). As for intensities, the change is more subtle, i.e. some bands remain practically unchanged, some become weaker and the others become stronger. For example, Moreira *et al.* [51] stated that the intensities, positions, and widths of BMN Raman modes vary with Ts. Moreover, the number of Raman modes can change due to different Ts. According to Wei *et al.* [93], with the increase in the Ts, the bands of the Raman spectra become narrower with blue-shift. Moreover, the number of modes increases with increasing Ts, and similar results were proved in other samples such as Ba[(Ni$_{0.7}$Zn$_{0.3}$)$_{1/3}$Nb$_{2/3}$]O$_3$ (BZNN) [91], Ba[Zn$_{1/3}$(Nb$_{0.4}$Ta$_{0.6}$)]O$_3$ (BZNT) [92] and BS$_{32}$ZN [94], i.e. the characteristics of Raman modes, including intensities, frequencies, and FWHM values can change with different Ts.

The long-range order degree can be evaluated by analysing Raman data in any $A(B'_{1/3}B''_{2/3})O_3$-type MWDC, which shows a strong dependence on the structural evolution of the ceramics at different sintering processes. Research on the BZNN ceramic [91] shows that the appearance of $F_{2g}$ modes indicates the long-range ordering of the samples and the lowest FWHM value of $A_{1g}$(Nb) modes indicates the highest ordering. The appearance of the extra phonon mode may be on account of the titling of the normal cubic cell.

The structural change verified with Ts in BZNT ceramics was evaluated by the Raman spectrum as shown in Fig. 5a. After fitted by the Lorentzian model, ten Raman modes exist in BZNT ceramics sintered at 1450°C, while 11 and 12 Raman modes appear in BZNT ceramics sintered at 1500 and 1550°C, respectively. The 1:2 ordering related mode of $E_g$(Nb/Ta) at about 220 cm$^{-1}$ disappear in the BZNT sample sintered at 1450°C, which presents that the crystal structure of the latter belongs to cubic ($Pm\bar{3}m$) perovskite with the 1:1 ordered structure.

The $F_{2g}$(Ba) modes are split into $A_{1g}$(Ba) and $E_g$(Ba) modes, as shown in Fig. 5b, indicating the BZNT ceramics possess a 1:2 order. The mode intensities decrease with increasing $T_s$, indicating the local symmetry increasing, accordingly. No splitting exists in the $F_{2g}$(O) modes, indicating the $A_{1g}$(O) and $E_g$(O) modes always overlapped, which can be well assigned according to the Lorentzian fitting results.

Notably, at least three novel Raman modes can be observed, which were also seen by Dias [81] and Nagai [37] in the BSZN and BSMT ceramics, respectively, due to the effect of the phase transition, i.e. distortion from the normal hexagonal cell to monoclinic phase with antiphase tilting of the oxygen octahedron.

The octahedral distortion is caused by the asymmetry of the O bonding network and cooperated by the second-order Jahn–Teller deformation of the $d_0$ Nb$^{5+}$ and Ta$^{5+}$ cations [31], i.e. the local symmetry decreases with increasing Ts, and the Raman mode number increases accordingly with the decrease in the intensities of the splitting peaks, which are also proved in BS$_{32}$ZN ceramics [94].

Just like Ts, sintering time (or soaking time) also has great influence on microwave dielectric properties and Raman modes in the frequencies, FWHW values, intensities, and number. Take BMT and BZN as examples. In Chen's work [49], the longer the sintering time, the larger the frequencies and the smaller the FWHM values of the BMT materials, i.e. the Raman shift and FWHW values are greatly affected by sintering time.

### 3.4 Correlation between Raman modes and microwave dielectric properties

Active Raman modes are non-polarised modes and related to the crystal structures, and generally speaking, no direct relation is determined between Raman spectra and microwave dielectric properties. However, the optical study shows that the 1:2 ordered phonons are closely correlated with the dielectric properties. The stretch modes of oxygen octahedron indicate the properties, i.e. the characteristics of Raman peaks have an indirect correlation with the properties, which were proved by BMT [48] and BMT–BMN [72].

To further know more about the mechanism of the microwave dielectric properties, it is necessary to determine the correlation between crystal structures and properties thorough knowledge on lattice vibrational characteristics, which contributes to design new MWDCs with excellent microwave dielectric properties. However, it is quite difficult to elucidate the relationship between atomic vibration and dielectric properties. The Raman spectra provide the correlation between vibration characteristics and the properties, even though the Raman phonons are of non-polarised modes [88, 95–97]. Based on the Raman shifts and FWHM values of the vibration modes, the relation between the phonon modes and the dielectric properties can be identified.

*3.4.1 $A_{1g}$(O) modes:* The oxygen octahedral stretch modes ($A_{1g}$(O)) at about 720–800 cm$^{-1}$ can exhibit microwave dielectric properties [49, 72]. Webb [88] proved the permittivities have a relationship with the wave numbers (frequencies) because the Raman shifts of $A_{1g}$(O) modes respond to the oxygen octahedron rigidity. An inverse relationship with Raman shifts of $A_{1g}$(O) phonon modes and dielectric constants were observed in Ba[Mg$_{(1-x)/3}$Zr$_x$Ta$_{2(1-x)/3}$]O$_3$ (BMZrT) [83], i.e. higher polarisability corresponds to a lower Raman shift.

Chia's result indicates that the quality of the oxygen-octahedron structure can be characterised by the FWHM of $A_{1g}$(O) stretch phonons, which is related to the $Q \times f$ value significantly [72], i.e. an inverse correlation between the FWHM value of $A_{1g}$(O) and $Q \times f$ value for the $x$BMT-$(1-x)$ BMN ceramics. An opposite variation trend for the width of the $A_{1g}$(O) mode and the $\tau_c$was also observed in BSZN ceramics [52], but a positive variation trend for Raman shift of the $A_{1g}$(O) mode and the $\tau_c$ value was observed in BMZrT [83]. Similar results are proved by the studies in BMT [48], Ba(Co$_{1/3}$Nb$_{2/3}$)O$_3$[53], Ba[Mg$_{(1-x)/3}$Zr$_x$Nb$_{2(1-x)/3}$]O$_3$ (BMZrN) [84], BZNN [91], and Ba(Zn$_{1/3}$Nb$_{2/3}$)O$_3$- CaTiO$_3$ [97], i.e. the shifts and the $A_{1g}$(O) width reflect the dielectric constants, the $\tau_c$ values and the $Q \times f$ values in the 1:2 ordered ceramics, which implies that the oxygen octahedron can reflect the microwave properties of MWDCs.

*3.4.2 $F_{2g}$(Ba, Sr) mode:* The lowest frequency mode $F_{2g}$(Ba, Sr) at about 105 cm$^{-1}$is generated by the lattice vibrations of Ba$^{2+}$/Sr$^{2+}$ ions in the A-site, which can be divided into $A_{1g} + E_g$ ($F_{2g} = A_{1g} + E_g$) when the crystal symmetry of ceramics is cubic perovskite (higher symmetry) and cannot split with lower symmetry of the
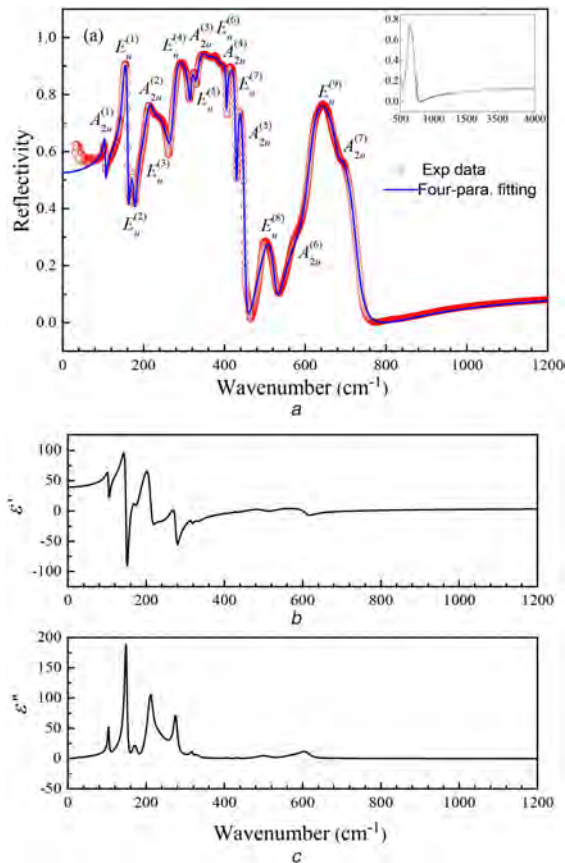
**Fig. 6** *Fitting results for the IR reflectance spectrum of BMN*
*(a)* Measured spectrum (circles) and the fitted curve (line), *(b)* $\varepsilon'$ spectrum and *(c)* $\varepsilon''$ spectrum [73]

ceramics having the 1:2 ordered structure. The $Ba^{2+}/Sr^{2+}$ ions are located in the gap of eight-oxygen octahedron and surrounded by 12-equidistant oxygen, thus their vibrations can affect the tilting of oxygen octahedron greatly. Therefore, the vibration modes in the A-site can be related to the dielectric properties indirectly. The Raman shift of the $F_{2g}(Ba,Sr)$ mode has a negative correlation with the dielectric constant and FWHM value of the $F_{2g}(Ba,Sr)$ mode has the positive correlation with the $\tau_c$ value, [52], i.e. the rigid $F_{2g}(Ba,Sr)$ mode correlates with the permittivity and $\tau_c$ values.

*3.4.3 1:2 ordered structure-related modes:* The modes between 150 and $-300$ cm$^{-1}$ are related to 1:2 ordered structures, which have a close relationship with the dielectric properties. Take $x$BMT–$(1-x)$BMN as an example [72]. The permittivities and Raman shifts of $A_{1g}(Ta/Nb)$ and $E_g(Ta/Nb)$ phones have a linear change with the increase of Ta, i.e. there is a positive relationship between the permittivities and the Raman shifts of $A_{1g}(Ta/Nb)$ and $E_g(Ta/Nb)$ modes. For $x = 0.5$, the widths of the $A_{1g}(Ta/Nb)$ and $E_g(Ta/Nb)$ modes were broadened and the $Q \times f$ values were lowered, i.e. there exists an inverse correlation between $Q \times f$ and FWHM values of $A_{1g}(Ta/Nb)$ and $E_g(Ta/Nb)$.

For BZNN ceramics, $\varepsilon_r$ is reverse with the FWHMs of $E_g(O)$ modes, $\tau_c$ has a negative correlation with the Raman shifts of $E_g(O)$ modes, and the change of tan $\delta$ is closely correlated with the FWHM values of $E_g(O)$ modes [91], which were also proved in BS$_{32}$ZN [94] and BMZrN [84].

In conclusion, the dielectric constant is closely correlated with Raman shifts of the $A_{1g}(O)$ modes and the FWHM values of the $F_{2g}(O)/E_g(O)$ modes. The $Q \times f$ and $\tau_c$ of MWDCs with 1:2 ordered structures can be characterised by the FWHM value of $A_{1g}(O)$ mode. The dielectric loss values have a close connection with the FWHM values of $A_{1g}(O)/E_g(O)$ active modes. The increase in the FWHM values of Raman modes is related to low bond-stretching

modes. The FWHM values of $A_{1g}(O)$ phonons show the the quality of oxygen-octahedron structures, which is highly corresponded with the $Q \times f$ values, i.e. $Q \times f$ values are influenced by the tetravalent-cation bond characteristics of the oxygen octahedron. $Q \times f$ values are also correlated with the FWHM values of $E_g(O)$ modes, which reflected the vibration of ordered structures. The rigid $F_{2g}(Ba,Sr)$ mode in the A-site substituted solid solutions correlates with the stable temperature coefficient of capacitance, which is also correlated with the Raman shifts of $E_g(O)$ modes and the FWHMs/frequencies of $A_{1g}(O)$ modes.

## 4  FIR phonon mode characteristics of MWDCs

To further explore the influence of the polar lattice phonons on the microwave dielectric properties, IR reflection modes caused by the absorption of the polar lattice vibration are necessary and can enable people completely understand the lattice vibrations [73, 98]. However, it is quite complicated to assign all the IR-active peaks since the resonant modes are highly diffused, and those modes of some MWDCs have been analysed by classical dispersion theory [95, 99].

For the ABO$_3$ cubic perovskite structure, there are three triply degenerate IR modes of $F_{1u}$ symmetry and one optically silent mode of $F_{2u}$ symmetry predicted by group theory, which are commonly called as the external modes (the BO$_6$ octahedron vibrates against A-site atom), the bending mode (B–O bond angle modulation), and the stretching mode (B–O bond-length modulation). As for paraelectric perovskites, the A–[BO]$_6$ external mode appears in the frequency <160 cm$^{-1}$, the B–O bending mode at 160–300 cm$^{-1}$ and the O–B–O stretching mode at 500–700 cm$^{-1}$ [99]. Generally speaking, the IR active modes between 150 and 500 cm$^{-1}$ are correlated with cation ordering and octahedral tilting. 16 IR active modes ($7A_{2u}$ and $9E_u$) appear, which are predicted by the factor group in the 1:2 ordered structure with the trigonal $P\bar{3}m1$ space group [46].

### 4.1 Assignment and illustration of FIR phonon modes

Simple cubic perovskites, such as SrTiO$_3$, present three or four IR modes, while complex perovskites such as BZN with the same cubic structure possess more IR modes [100]. As for $Sr(Zn_{1/3}Nb_{2/3})O_3$ and $Sr(Mg_{1/3}Nb_{2/3})O_3$ (SMN), the visualised IR spectra are well fitted by 13 and 20 phonons [100], respectively.

Group theoretical analysis for the Brillouin-zone-centre vibrations of BMT ceramics with the $D_{3D}^3$ structure causes the irreducible representations with $7A_{2u}$ (*c*-axis polarised) $+9E_u$ (the *ab*-plane polarised) IR vibration modes [56]. However, only 15 IR peaks are identifiable [49], and the last one is undetected because the peak is either too weak or overlaps with other modes.

BZT has 18 IR-active modes, including $A_{2u}$ and $E_u$ modes. As one of the $A_{2u}$ modes and one of the $E_u$ modes correspond to the uniform displacements of ions, which do not change their relative positions at all. Therefore, the number of IR-active modes is 16 at most. In [71, 99], 14 resonant modes were observed for BZT.

The IR-active modes of the BMN, which were studied by Diao *et al.* [73], were assigned with the assistance of the FPSQ fitting and the mode frequency sequence calculated using first-principle calculation. Fig. 6*a* shows the experimental and calculated reflectivity of BMN, Figs. 6*b* and *c* show the frequency dependencies of real and imaginary parts of the permittivity, respectively.

The symmetry assignments to the FIR spectrum of the BMN were also conducted by Liu [80, 101] based on the first-principle calculation. Most of the assignments are identical to those in the present study, except for the modes $E_u^{(6)}$ and $A_{2u}^{(4)}$. Given the significantly closed frequencies, the calculation deviations of the assignments for these two modes are swapped with respect to those in Liu *et al.* [80, 102].

To verify the contributions of the vibrational modes to the dielectric properties, the permittivity $\varepsilon_j$, and loss tan $\delta_i/\omega$ were

**Table 3** Parameters of the IR-active modes for the FPSQ model [73]

| No. | Modes | $f_{thoe}$, cm$^{-1}$ | Int., km/mol | $\Omega_{jTO}$, cm$^{-1}$ | $\gamma_{jTO}$, cm$^{-1}$ | $\Omega_{jLO}$, cm$^{-1}$ | $\gamma_{jLO}$, cm$^{-1}$ | $\varepsilon_j$ | $\tan\delta_j/\omega$, $10^{-17}$/Hz |
|---|---|---|---|---|---|---|---|---|---|
| 1 | $A_{2u}^{(1)}$ | 93.1 | 6.80 | 104.2 | 4.5 | 105.9 | 3.5 | 1.7782 | 1.1288 |
| 2 | $E_u^{(1)}$ | 103.3 | 0.74 | 149.2 | 8.0 | 161.4 | 4.2 | 10.1912 | 2.3255 |
| 3 | $E_u^{(2)}$ | 112.2 | 49.72 | 173.6 | 19.4 | 177.6 | 8.6 | 1.7738 | 0.7101 |
| 4 | $A_{2u}^{(2)}$ | 121.9 | 18.86 | 212.0 | 18.4 | 220.1 | 24.7 | 12.8573 | 2.0765 |
| 5 | $E_u^{(3)}$ | 130.4 | 0.012 | 222.6 | 51.1 | 266.0 | 28.2 | 3.6739 | 1.4290 |
| 6 | $E_u^{(4)}$ | 181.3 | 29.79 | 276.0 | 11.9 | 315.8 | 9.3 | 2.1136 | 0.1632 |
| 7 | $E_u^{(5)}$ | 219.6 | 24.20 | 316.9 | 7.4 | 330.2 | 19.9 | 0.1073 | 0.0047 |
| 8 | $A_{2u}^{(3)}$ | 269.5 | 49.53 | 332.6 | 16.9 | 362.8 | 56.4 | 0.1992 | 0.0222 |
| 9 | $E_u^{(6)}$ | 371.8 | 0.0048 | 366.9 | 52.9 | 387.1 | 56.2 | 0.1814 | 0.0713 |
| 10 | $A_{2u}^{(4)}$ | 387.9 | 0.0099 | 390.9 | 70.3 | 404.6 | 3.8 | 0.1353 | 0.0647 |
| 11 | $E_u^{(7)}$ | 451.4 | 1.095 | 405.0 | 4.3 | 428.6 | 5.9 | 0.0123 | 0.0004 |
| 12 | $A_{2u}^{(5)}$ | 476.1 | 7.34 | 430.6 | 7.4 | 451.1 | 7.6 | 0.0238 | 0.0012 |
| 13 | $E_u^{(8)}$ | 496.2 | 20.098 | 501.4 | 52.7 | 526.4 | 22.0 | 0.5300 | 0.1455 |
| 14 | $A_{2u}^{(6)}$ | 577.5 | 51.25 | 554.4 | 89.7 | 603.4 | 111.2 | 0.6281 | 0.2749 |
| 15 | $E_u^{(9)}$ | 649.4 | 32.50 | 609.7 | 32.3 | 681.3 | 25.4 | 0.0916 | 0.0134 |
| 16 | $A_{2u}^{(7)}$ | 805.1 | 2.42 | 683.0 | 25.3 | 729.5 | 29.3 | 0.0054 | 0.0006 |

calculated. The results (Table 3) imply that the IR-active modes at lower frequencies have larger $\varepsilon_j$ and $\tan\delta_i/\omega$, particularly the $E_u^{(1)}$ modes at 149 cm$^{-1}$ and the $A_{2u}^{(2)}$ mode at 212 cm$^{-1}$, which have larger values of $\varepsilon_j$ and $\tan\delta_i/\omega$ than the other modes, indicating that these two modes have larger contributions to the permittivity and dielectric loss, and the vibrations related to the NbO$_6$ octahedron have more contributions to the IR-active modes and the microwave dielectric properties than those related to the MgO$_6$ octahedron, i.e. the dielectric properties may be more sensitive to the doping in the Nb site than in the Mg site.

For the IR reflectivity spectra, the assignments for most modes are identical. However, given the calculation deviations and the close peak frequencies, the assignments for a few modes are vague, e.g. the assignments for the modes $E_u^{(2)}$ and $A_{2u}^{(2)}$, as well as $E_u^{(6)}$ and $A_{2u}^{(4)}$ in BMN, are swapped as compared with those in BMT. In addition, the correlated modes of BMT and BMN have different contributions to the microwave dielectric properties, e.g. in BMT, the $E_u^{(4)}$ and $E_u^{(5)}$ modes have the largest contributions, whereas, in BMN, the largest contributions come from the $E_u^{(1)}$ and $A_{2u}^{(2)}$ modes. The vibration frequencies of TO and LO modes, such as $Q_{jTO}$ and $Q_{jLO}$ for BMT [56] and Ba([Mg$_{1-x}$Zn$_x$]$_{1/3}$Ta$_{2/3}$)O$_3$ [100] ceramics in the FIR region were also calculated by four-parameter semiquantum model (FPSM).

IR reflectivity spectra of solid solution ceramics can be divided into three parts, as stated above and take the BSZN ceramics as an example [52]. The spectra of BSZN possess 11 IR modes, and the frequencies were determined as 140, 151, 224, 240, 275, 315, 412, 435, 460, 525, and 629 cm$^{-1}$, respectively [52]. The splitting and strengthening of the low-frequency phonons mode are related to the vibrations of Ba$^{2+}$/Sr$^{2+}$ against the BO$_6$ octahedron (part I). The bands at 180–300 cm$^{-1}$ belong to the B–O bending modes and the modes above 500 cm$^{-1}$ are indexed as O–B–O stretching modes. The damped modes are related to vibrations of Zn$^{2+}$/Nb$^{5+}$, which have a great effect on the B-site disordered structure. Similar results can also be proved by other methods proposed in [43, 60, 85, 98, 103, 104] substituted in B-sites, which leads to a change in number, frequencies, and intensities of the reflection bands.

New polar mode occurs at about 150 cm$^{-1}$ where $x \geq 0.65$ for BSZN in comparison with single-phase BZN, which was similar to the results of Nagai et al. [37]. Brillouin zone folding and phase transition are two possible reasons, and the latter is caused by the ordered phase with the antiphase tilting of the oxygen octahedron

[41]. The change in the number of bands was also found in the BMZrT ceramics, i.e. three active modes exist for the samples where $x = 0$, 0.05: about 158 cm$^{-1}$ of $E_g$(O), 210 cm$^{-1}$ of $E_g$(Ta), and 263 cm$^{-1}$ of $A_{1g}$(Ta), which have been assigned as the 1:2 ordered structure-related vibrations, however, for the samples where $x = 0.05$, the modes $E_g$(Ta) and $A_{1g}$(Ta) decrease in intensities, i.e. the degree of 1:2 ordered phase decreases. When $x = 0.10$, 0.20, and 0.30, all of these three modes disappear, which reflects non-existence of the 1:2 ordered structures, implying the crystal structures changed with increasing Zr$^{4+}$ concentration [98], i.e. the introduction of different atoms in the A/B-site promotes the loss of both translation and inversion symmetry, which leads to the appearing/disappearing of the additional modes [55].

Polar modes of the Ba[Sn$_x$Zn$_{(1-x)/3}$Nb$_{2(1-x)/3}$]O$_3$ (BSnZN) ceramics [95] at about 475 cm$^{-1}$ shift to lower frequencies with increasing Sn$^{4+}$ content, and the change in band intensities was also observed in BSZN, BSnZN, Ba([Mg$_{1-x}$Zn$_x$]$_{1/3}$,Ta$_{2/3}$)O$_3$ (BMZT), BZNT and BMZrN ceramics [103, 104]. The phase transformation results in the modification of the polar modes.

In brief, the FIR spectra of the $A(B'_{1/3}B''_{2/3})O_3$-type MWDCs include three parts: the vibration of A-site ions against the BO$_6$ octahedron, the vibration related to the B–O bending modes, and the vibration related to the O–B–O stretching modes. Lattice vibrations are sensitive for material substitution and FIR spectra give much information for the lattice vibrations. The intensities, number, and positions of the reflection bands change with different ions.

### 4.2 Calculation of microwave dielectric properties from FIR spectra

FIR dielectric dispersion of the perovskites was comprehensively investigated in the 1960s [105, 106]. The FIR spectroscopy reflects polarisation with respect to the electromagnetic field (IR), thus strongly and directly relates to the microwave dielectric properties [49], which can be estimated by the dispersion parameters (frequencies and damping constants) to judge the characteristics of the crystal structures obtained by three spectrum fitting methods based on the classical dispersion theory [101], including Kramers–Krönig (K–K) analysis, Lorentz three-parameter classical and FPSQ. The origin and physical mechanism of the microwave dielectric properties can be obtained from lattice vibrational spectra.

*4.2.1 K–K analysis:* The K–K dispersion relation is a method to estimate optical and dielectric characteristics of ceramics by reflectance data measured at the incidence of 45°, which needs only a certain reflectance spectrum and is effective for either polarised or completely unpolarised incident light

$$n = \frac{1-R}{1+R-2\cos\sqrt{R}}, \tag{15}$$

$$k = \frac{-2\sin\sqrt{R}}{1+R-2\cos\sqrt{R}}. \tag{16}$$

The angle $\theta$ is the phase change on reflection, and by knowing $R(\omega_c)$ and $\theta(\omega_c)$, $n$ and $R$ can be calculated from (15) and (16) [107]. The value of $\theta$ at any frequency $\omega_c$ is not isolated, while it is directly interrelated with the reflection spectra by the integral transform.

$$\varphi(\omega_c) = \frac{1}{\pi}\int_0^\infty \ln\left|\frac{\omega+\omega_c}{\omega-\omega_c}\right|\frac{d\ln\{R(\omega)\}^{1/2}}{d\omega}d\omega. \tag{17}$$

The dependence of reflectance upon $\varphi$ (the angle of incidence) is very critical for certain values of $k$ and indeed forms the basis of a method for evaluating $n$ and $k$ [108]. This transform is called K–K dispersion relations by Robinson [107]. Therefore, the reflectance $R$ at normal incidence as a function of frequency is the only experimental measurement required [109, 110].

As for K–K analysis to MWDCs, the Lorentz distribution of the TO modes should be used to fit the spectra, from which the microwave dielectric properties ($\omega_{0j}^2 \gg \omega^2$) can be calculated using dispersion functions [49, 73]. $\varepsilon'$ and $\varepsilon''$ are real parts and imaginary parts of complex dielectric constants, $\varepsilon = \varepsilon' + i\varepsilon''$, which can be derived from FIR spectra using K–K analysis

$$\varepsilon'' = 2nk = \sum_j\left(\frac{4\pi e^2 N_j}{mV}\right)\frac{r_j\omega^2}{(\omega_{0j}^2-\omega^2)^2+\gamma_j^2\omega^2}, \tag{18}$$

$$\varepsilon' = n^2-k^2 = \varepsilon_\infty + \sum_j\left(\frac{4\pi e^2 N_j}{mV}\right)\frac{1}{\omega_{0j}^2} = \varepsilon_\infty + \sum_j 4\pi\rho_j, \tag{19}$$

$$\frac{1}{Q} = \frac{\varepsilon''}{\varepsilon'} = \sum_i\frac{4\pi\rho_j\gamma_j\omega}{\omega_{0j}^2\varepsilon'}, \tag{20}$$

where $N_j$ and $\gamma_j$ are the numbers of charges bound with the resonators of the frequency $\omega_{0j}$ and the associated damping coefficient, respectively; $m$ is the mass and $V$ is the volume. The summation is over the $j$th modes in the spectrum, and $\infty$ is the optical permittivity. The relationship between resonant strength $(4\pi\rho_j)$ and resonance frequency $(\omega_{0j})$ originates from the ionnic bonding strength and the displacements of the ions. $Q \times \omega$ is a constant under the $\omega_{0j}^2 \gg \omega^2$ approximation at microwave frequencies [49].

The important parameters in (19), $\omega_{0j}$, $\gamma_j$, and $4\pi\rho_j$ can be obtained from the fitting of the FIR to calculate the microwave dielectric response, and next perform the correlation with the dielectric properties. The resonant frequency $(\omega_{0j})$ correlates with the strength of $B''$–O or $B'$–O mode, which relates to the $B''$–O or $B'$–O dipoles polarisability, i.e. the dielectric constants, accordingly. Damping coefficient $(\gamma_j)$ of the vibrational modes has a positive relationship with the coherency of $B''$-layer or O-layer vibration and hence correlates with the dielectric loss [48].

The FIR spectra, which are processed using the K – K relationship, was found to well explain microwave dielectric properties of the $A(B'_{1/3}B''_{2/3})O_3$-type MWDCs. Furthermore, the THz dielectric properties of MWDCs can also be extrapolated from the FIR spectra using the same method. Dielectric properties were calculated according to dispersion parameters: (i) resonance frequency $(\omega_{0j})$ correlates with the dielectric constant and (ii) damping coefficient $(\gamma_j)$ relates to the dielectric loss, i.e. K–K

analysis can be used to predict the dielectric constants and dispersion parameters of $A(B'_{1/3}B''_{2/3})O_3$-type MWDCs, such as BMT [48], BZT [71, 110], BSZN [52], $(Ba_{1-dx}Sr_x)(Zn_{1/3}Ta_{2/3})O_3$ [111], $Ba[(Zn_{0.2}Mg_{0.8})_{1/3}Nb_{2/3}]O_3$ (BZMN) [43], $x$BMT-$(1-x)$BMN [49], and BSnZN [95].

For each composition, the fitting of the reflectivity spectra allows people to evaluate the imaginary part of the permittivity $\varepsilon''$, which were carried out on the maximum of the obtained interference patterns in the IR frequency range. The imaginary part presents the absorption characteristics of the vibrator to the electromagnetic wave.

For single-phase MWDCs with $P\bar{3}m1$ symmetry, such as BMT ceramics, 16 IR active modes are predicted, i.e. $7A_{2u}+9E_u$. The modes $<300$ cm$^{-1}$ possess large resonance strength $(4\pi\rho_j)$ [112], which can influence the properties of the BMT. The resonance frequency $(\omega_{0j})$ correlates with the strength of Ta–O/Mg–O bond, i.e. the polarisability of the $B''$–O/$B'$–O dipole, therefore relates to the permittivity, just as stated above.

As for the paraelectric perovskites, $A$–$BO_3$ external and $O$–$B$–$O$ bending modes are two low-frequency modes, which have the major influence on the real parts of the dielectric constants [111], i.e. the higher dielectric strength is caused by the Ba–$BO_3$ external vibration, O–$B''$–O and O–$B'$–O bending vibrations, while the $B''O_6$ and $B'O_6$ stretching vibrations have the lowest contribution.

For the ceramic with substitution in the A site, take BSZN solid solution ceramics as an example. An approximation of a transverse optic frequency, $\omega_{TO}$, of a polar mode (vibrator) is obtained as the resonant frequency where $\varepsilon''$ reaches a maximum value [52, 81]. Through the Lorentz fitting method, every frequency of the $\varepsilon''$ peaks can be achieved with the increasing substitution ions. The peak frequencies shift with the Sr$^{2+}$ content relates to the variation of polar modes for the TO frequencies and take on a nonlinear change.

According to the previous results of the BZMN ceramics, the increase in the TO-phonon damping, i.e. broadening of the reflection bands, was caused by the substitution for Zn$^{2+}$ by Mg$^{2+}$ in the $B'$-site [43]. The frequency shift of each peak in the BZMN ceramics is similar to that in BSZN [52]. The variation of peak frequencies implies that phonon modes change in a sensitive and unusual way depending on the crystal structures. The peak frequencies shift relates to the change in the TO frequencies, and five distinct modes are present at $x \le 0.6$, however, one mode disappears at $x > 0.6$, implying a phase transition.

The results of ceramics substituted in $B''$-site ions, just like BZNT [103], show that the lattice vibration at low frequency deeply influences their microwave dielectric properties, which is similar as reported by Tamura [71], Wakino [99], and Shimada [101].

*4.2.2 Lorentz three-parameter classical model:* The Lorentz three-parameter classical model describes the relationship between the complex permittivity $(\varepsilon^*)$ and the vibrational modes of the materials as

$$\varepsilon^*(\omega) = \varepsilon'(\omega) - i\varepsilon''(\omega) = \varepsilon_\infty + \sum_{j=1}^m\frac{\Omega_j^2 S_j}{\Omega_j^2-\omega^2+i\omega\gamma_j}, \tag{21}$$

where $S_j$, $\Omega_j$, and $\gamma_j$ are the strength, eigenfrequency, and damping factor of the $j$ vibrational mode, respectively, and $m$ is the number of vibrational modes [54]. Dielectric constant $\varepsilon_r$ and tan $\delta$ at certain microwave frequency can be calculated using the dispersion parameters

$$\varepsilon_r = \varepsilon_\infty + \sum_j 4\pi\rho_j, \tag{22}$$

$$\tan\delta = \frac{\sum_j 4\pi\rho_j(\gamma_j\omega)/\omega_j^2}{\varepsilon_\infty+\sum_j 4\pi\rho_j}, \tag{23}$$

where the strength $4\pi\rho_j$, width $\gamma_j$, and resonant frequency $\omega_j$ of each oscillator are called the dispersion parameters and permittivity $\varepsilon_\infty$ is caused by an electronic polarisation at optical frequency [71].

The Lorentz three-parameter classical model is obtained by superimposing a plurality of different vibration modes based on the classic 1D harmonic oscillator model (1D spring model). Compared with the K–K analysis, a classic vibration model ignores limit relations between the real and imaginary part of the permittivity and more adapted to complicated material systems [112]. The classical harmonic oscillator model can be written as [112]

$$\varepsilon(\omega) = \varepsilon_\infty - \sum \varepsilon_j(\omega) = \varepsilon_\infty + \sum \frac{\omega_j^2 S_j}{\omega_j^2 - \omega^2 + i\omega\Gamma_j}, \quad (24)$$

where $\omega_j$, $\Gamma_j$ and $S_j$ are the resonance frequency, the damping constant and the oscillator strength of the $j$th phonon, respectively. Different symbols between the Lorentz three-parameter classical model and classical harmonic oscillator model represent the same physical significance.

Studies on the classical harmonic oscillator model of the MWDCs have also been extensively investigated, such as the $ABO_4$ ceramics system [113, 114], i.e. ($Na_{0.5x}Bi_{1-0.5x}$)($Mo_xV_{1-x}$)$O_4$, [($Li_{0.5}Ln_{0.5})_{1-x}Ca_x$]$MoO_4$ (Ln = Sm and Nd), and $Ba(B'_{1/3}B''_{2/3})O_3$ ceramics system [115–117], i.e. BMT, BZT, $Ba(Mg,Sn,Ta)O_3$,$Ba(Zn,Zr,Ta)O_3$,$CaTiO_3$–SMN.

Wang et al. analysed the FIR reflection spectrum of $MgTiO_3$ by Lorentz three-parameter classical mode. The intrinsic properties were calculated: $\varepsilon_r = 14.9$, $Q_f = 258,000$ GHz, and the parameters ($S_j$, $\Omega_j$, and $\gamma_j$) for seven IR modes were obtained [54]. Tamura et al. analysed BZT by the Lorentz three-parameter classical model. Dielectric constant $\varepsilon_r$ and tan $\delta$ at the microwave frequency were calculated using the dispersion parameters above: $\varepsilon_r = 30.3$, $Q = 20,200$ (7 GHz) [71]. In Sawada's research [112], 15 observed phonons can be well fitted in reflectivity spectrum (Figs. 3 and 4) and five IR-active phonons of BMT ceramics with frequencies <280 cm$^{-1}$ have great influence on permittivity and dielectric loss.

Resonant frequencies of IR-active phonons rely on the angle between the electric field of the incident light and the direction of the crystal axis. Owing to the different resonant frequency in each grain, the reflection peaks of ceramics with many random oriented grains can be broadened, and thus present a large damping constant and a small $Q$ value [112].

The physical meaning of the three-parameter model is clear, and the mathematical treatment process is relatively simple. However, the interactions between different oscillators are not considered for the three-parameter model. As for FPSQ, its description is closer to the actual situation because the interaction between different oscillators is considered with a relatively complex mathematical process. In short, the damping factors $\gamma_j$ of the LO and TO modes are not considered in the three-parameter model, and therefore, the fitting curve of FPSQ is better than that of the three-parameter model.

*4.2.3 FPSQ model:* The FPSQ model, short for FPSQ, is another method to calculate the dielectric properties of MWDCs. The model presented by Gervais [118] can be used to convert the reflectivity data into dielectric data, and the frequency dependent complex dielectric function can be written as

$$\varepsilon^*(\omega) = \varepsilon'(\omega) - i\varepsilon''(\omega) = \varepsilon_\infty \prod_{j=1}^{n} \frac{\Omega_{jLO}^2 - \omega^2 + i\omega\gamma_{jLO}}{\Omega_{jTO}^2 - \omega^2 + i\omega\gamma_{jTO}}, \quad (25)$$

$$\Delta\varepsilon_j = \varepsilon_\infty \left(\frac{\Omega_{jLO}^2}{\Omega_{jTO}^2} - 1\right) \prod_{k \neq j} \frac{\Omega_{kLO}^2 - \Omega_{jLO}^2}{\Omega_{kTO}^2 - \Omega_{jTO}^2}, \quad (26)$$

$$\tan\delta_j = \frac{\Delta\varepsilon_j(\gamma_{jTO} \cdot \omega)\Omega_{jTO}^2}{\varepsilon_\infty + \sum_i \Delta\varepsilon_i} \propto \frac{\gamma_{jTO} \cdot \omega}{\Omega_{jTO}^2}, \quad (27)$$

where $\Omega_{jTO}$, $\gamma_{jTO}$, and $\Omega_{jLO}$, $\gamma_{jLO}$are the frequencies and damping factors of the $j$th transverse and longitude modes of vibration, respectively. The measured IR reflectance spectrum can be fitted giving up to $n$ pairs of TO–LO modes.

The IR-active modes of the BMN, which were studied by Diao et al. [73], were assigned with the assistance of the FPSQ fitting and the mode frequency sequence calculated using the first-principle calculation. The symmetry assignments to the FIR spectrum of BMN were also conducted by Liu [80, 102] based on the first-principle calculation. Most of the assignments are identical to those in the present study, except for the modes $E_u^{(6)}$ and $A_{2u}^{(4)}$. Given the significantly close frequencies, the calculation deviations of the assignments for these two modes are swapped with respect to those in Liu et al. [80, 102].

To verify the contributions of the vibrational modes to the microwave dielectric properties, the permittivity $\varepsilon_j$ and loss tan $\delta_i/\omega$were calculated by (26) and (27), respectively. The calculated data imply that the IR-active modes at lower frequencies have larger $\varepsilon_j$ and tan $\delta_i/\omega$, particularly the $E_u^{(1)}$ modes at 149 cm$^{-1}$ and the $A_{2u}^{(2)}$ mode at 212 cm$^{-1}$, which have larger values of $\varepsilon_j$ and tan $\delta_i/\omega$ than the other modes, indicating that these two modes have larger contributions to the permittivity and dielectric loss, and the vibrations related to the $NbO_6$ octahedron have more contributions to the IR-active modes and the microwave dielectric properties than those related to the $MgO_6$ octahedron, i.e. the dielectric properties may be more sensitive to doping in the Nb site than doping in the Mg site.

For the IR reflectivity spectra, the assignments for most modes are identical. However, given the calculation deviations and the close peak frequencies, the assignments for a few modes are vague, e.g. the assignments for the modes $E_u^{(2)}$ and $A_{2u}^{(2)}$, as well as $E_u^{(6)}$ and $A_{2u}^{(4)}$ in BMN, are swapped as compared with those in BMT. In addition, the correlated modes of BMT and BMN have different contributions to the microwave dielectric properties, e.g. in BMT, the $E_u^{(4)}$ and $E_u^{(5)}$ modes have the largest contributions, whereas, in BMN, the largest contributions come from the $E_u^{(1)}$ and $A_{2u}^{(2)}$ modes. The vibration frequency of TO and LO modes, such as $Q_{jTO}$ and $Q_{jLO}$ for BMT [56] and BMZT [101] ceramics in the FIR region were also calculated by FPSM.

### 4.3 Effect of processing conditions on FIR phonon modes of MWDCs

The processing condition, such as sintering temperature (Ts) and sintering time, can greatly influence the crystal structures and microwave dielectric properties, and accordingly, have an influence on the FIR modes of MWDCs, i.e. there exists variation in the intensities, the FWHM values and the frequencies of the FIR spectra due to different processing conditions, especially Ts.

Take the $Ba_{0.3}Sr_{0.7}[(Zn_{0.4}Mg_{0.6})_{1/3}Nb_{2/3}]O_3$ (BSZMN) solid solutions as an example [119], whose FIR reflectivity spectra are shown in Fig. 7. All of the FIR reflectivity bands are transferred to lower frequencies as Ts increases, and the intensities of some reflectivity bands also vary with the increasing Ts, i.e. broadening of bands near 140 cm$^{-1}$ in the region (I) and the strength drop of the bands near 550 cm$^{-1}$ in the third region (III), which indicate that the increase in the Ts causes an increase in the phonon damping in the BSZMN solid solutions. In the second region (II), the intensities of the weak peaks increase with the increasing Ts, which indicates the ordering degree increasing.

The bands of the BZMN ceramics near 150 cm$^{-1}$ increase in intensities with increasing Ts, which is similar to the results of $BSn_{32}ZN$ ceramics [95], whose polar modes near 240 cm$^{-1}$ become larger in FWHM values with increasing Ts. The polar modes at about 660 cm$^{-1}$ shift to low frequency and the intensities becomes weak as Ts increasing. Similar results can be obtained in BZMN ceramics: as intensities increase in the bands near 150 cm$^{-1}$ with increasing Ts in the range of 50–200 cm$^{-1}$ [93], which indicates a decrease in the phonon damping and demonstrates that
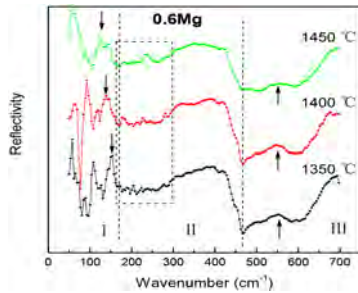
**Fig. 7** *FIR reflectivity spectra of the BSZMN solid solutions sintered [119]*

the complex nature of the atoms in the B-site promotes the splitting of the vibrational modes, leading to a more complicated IR spectrum.

In conclusion, the modes vary in shape (FWHM and overlapping), intensity, position (frequency shift) and number (additional modes) with the variation of Ts and sintering time significantly, and FIR reflectivity bands shift to a lower frequency with increasing Ts. In other words, the processing condition significantly affected the phonon parameter characteristics because of the phase transition and the second phase, especially Ts.

### 4.4 Relationship of FIR modes with crystal structures

Traditionally, the IR reflection bands are derived from polar lattice vibration absorption. Most research studies have been focused on the relationship between IR-active phonon modes and microwave dielectric properties and few investigations refer to the influence of the crystal structures dependent on the crystal structures, and therefore, there exists a relationship between IR-active modes and crystal structures indirectly.

The tilting of the oxygen octahedron has a great influence on the crystal structures of MWDCs, and their microwave dielectric properties are affected accordingly [37–39]. Reaney *et al.* [40] discussed the relationship between $\tau_f$ and the tilting of the oxygen octahedron in the system of Ba- and Sr-based 1:2 ordered complex perovskite. Woodward [120] demonstrated the structural changes due to the tilting of the oxygen octahedron in the 1:1 ordered complex perovskite [37–40].

16 IR active modes ($7A_{2u}$ and $9E_u$) appear in the 1:2 ordered materials with the structure of the trigonal $P\bar{3}m1$ space group [85] predicted by the factor group. Generally speaking, the IR active modes between 150 and 500 cm$^{-1}$ have a connection with cation ordering and octahedral tilting [92], which can be supported in many different kinds of MWDCs.

Nagai *et al.* [37] analysed the correlation between the crystal structure and the phase transition of the BSMT materials, and an anomaly IR-active phonon mode was observed at around 300 cm$^{-1}$, which probably arise from the influence of the Brillouin zone folding and the phase transition, i.e. the new polar mode is attributed to the ordered phase with antiphase tilting of the oxygen octahedron [37, 41]. Nagai *et al.* also observed the appearance and splitting of phonon modes, arising from the structural phase transformation owning to oxygen octahedral tilting [37].

A similar phenomenon appears in the $(Ba_{0.3}Sr_{0.7})$ $[(Zn_xMg_{1-x})_{1/3}Nb_{2/3}]O_3$ (BSZMN, $x = 0.0, 0.2, 0.4, 0.6, 0.8, 1.0$) solid solution ceramics [85]. Extra IR active modes were observed near 300 cm$^{-1}$ ($x \le 0.2$), and 500 cm$^{-1}$ ($x \ge 0.8$). The former samples have 1:2 ordered hexagonal unit cells with an antiphase tilting of the oxygen octahedron, and the latter indicates that the crystal structures are of the transformed phases [85].

According to the above statement, there is an indirect relationship between IR-active phonon modes and crystal structures, especially tilting of the oxygen octahedron, ordered structures, and phase transition.

## 5 Conclusion

The review summarises the lattice dynamics and phonon characteristics of $A(B'_{1/3}B''_{2/3})O_3$-type MWDCs systemically in order

to introduce remarkable progress in this field and make a guide for designing the next advanced MWDCs. The concluding remarks are as follows:

(i) The basic theory of the lattice vibration was stated to show its meaning, function, and application to MWDCs, as well as the prediction of the number and type of vibrational modes by group theory analysis. The atomic sites and corresponding modes in Raman spectra and FIR reflection spectra were assigned and identified.

(ii) The relationship between Raman modes and crystal structures were established and stated. The modes vary in shape (the bands can change their sharp and overlap to each other), intensity, and position (frequency shift) with the variation of composition in A- and B-site. The effects of the processing conditions, such as Ts and time, as well as the ordered/disordered superstructures, on the vibrational modes were summarised systemically. The composition, sintering temperature, and time can affect the ordered structure significantly. The modes appearing in Raman spectra, which related to the 1:2 ordered structure – related vibrations, would increase in number and intensities with increasing Ts and time, i.e. the 1:2 ordered nano-regions grow with Ts and time.

(iii) The correlation between Raman modes and dielectric properties are presented and summarised. Although Raman modes are non-polar, some Raman modes are important on the dielectric properties. The dielectric constants $\varepsilon_r$ and the temperature coefficient of dielectric constants have a significant relationship with the Raman shifts, and the dielectric loss tan $\delta$ values are closely correlated to the FWHM values of the $A_{1g}$(Nb) and $E_g$(O) active modes. The Raman shifts of the $A_{1g}$(O) modes at 780 cm$^{-1}$ positively correlate with the temperature coefficient of dielectric constants and an inverse correlation with the dielectric constant, i.e. the concrete structure–property relationship can be established using lattice vibrational modes as the media.

(iv) The intrinsic properties can be evaluated by the dispersion parameters (frequencies and damping constants), three spectrum fitting methods on account of the classical dispersion theory, including K–K analysis, Lorentz three-parameter classical model and FPSQ. Their origin and physical mechanism can be obtained from lattice vibrational spectra.

(v) The substitution of different atoms in the B-site promotes the loss of both translational and inversion symmetry. Therefore, additional modes can be observed in the FIR spectrum. A slight change of the crystal structure sometimes leads to an abnormal shift of the modes in the FIR spectra. Although FIR modes are polarised modes, the relationship between FIR modes and crystal structures are also presented and summarised, i.e. the relationship between FIR active phonon modes and the crystal structures of $A(B'_{1/3}B''_{2/3})O_3$ ceramics can be established.

(vi) More detailed research about another type of MWDC, including the lattice dynamics and the first principle calculations, should be carried out to know their phonon characteristics, the lattice dynamics of the MWDCs is most important in the study of the structure–property relationship.

## 6 Acknowledgments

# 7 References

[1] Vanderah, T.A.: 'Talking ceramics', *Science*, 2002, **298**, pp. 1182–1184

[2] Qiao, H.Y., Sun, H.Q., Li, J.Z.*, et al.*: 'Structure, intrinsic properties and vibrational spectra of Pr(Mg$_{1/2}$Sn$_{1/2}$)O$_3$ ceramic crystal', *Sci. Rep.*, 2017, **7**, p. 13336

[3] Fan, X.C., Chen, X.M., Liu, X.Q.: 'Complex-permittivity measurement on high-Q materials via combined numerical approaches', *IEEE Trans. Microw. Theory*, 2005, **53**, pp. 3130–3134

[4] Fu, M.S., Liu, X.Q., Chen, X.M.*, et al.*: 'Effects of Mg substitution on microstructures and microwave dielectric properties of Ba(Zn$_{1/3}$Nb$_{2/3}$)O$_3$ perovskite ceramics', *J. Am. Ceram. Soc.*, 2010, **93**, pp. 787–795

[5] Cruickshank, D.: '1–2 GHz dielectrics and ferrites: overview and perspectives', *J. Eur. Ceram. Soc.*, 2003, **23**, pp. 2721–2726

[6] Wakino, K.: 'Miniaturization techniques of microwave components for mobile communications systems-using low loss dielectrics', *Ferroelectr. Rev.*, 2000, **2**, pp. 1–49

[7] Scott, R.I., Thomas, M., Hampson, C.: 'Development of low cost, high performance Ba(Zn$_{1/3}$Nb$_{2/3}$)O$_3$ based materials for microwave resonator applications', *J. Eur. Ceram. Soc.*, 2003, **23**, pp. 2467–2471

[8] Reaney, I.M., Iddles, D.: 'Microwave dielectric ceramics for resonators and filters in mobile phone networks', *J. Am. Ceram. Soc.*, 2006, **89**, pp. 2063–2072

[9] Freer, R., Azough, F.: 'Microstructural engineering of microwave dielectric ceramics', *J. Eur. Ceram. Soc.*, 2008, **28**, pp. 1433–1441

[10] Sebastian, M.T., Jantunen, H.: 'Low loss dielectric materials for LTCC applications: a review', *Int. Mater. Rev.*, 2008, **53**, pp. 57–90

[11] Richtmyer, R.D.: 'Dielectric resonators', *J. Appl. Phys.*, 1939, **10**, pp. 391–398

[12] Xu, Y., Chen, X.M., Wang, L.: 'Sol–gel preparation of BaTi$_4$O$_9$ and Ba$_2$Ti$_9$O$_{20}$', *J. Am. Ceram. Soc.*, 2001, **84**, pp. 669–671

[13] Liu, B., Li, L., Liu, X.Q.*, et al.*: 'Structural evolution of SrLaAl$_{1-x}$(Zn$_{0.5}$Ti$_{0.5}$)$_x$O$_4$ ceramics and effects on their microwave dielectric properties', *J. Mater. Chem. C*, 2016, **4**, (21), pp. 4684–4691

[14] Xiang, H.C., Fang, L., Fang, W.S.*, et al.*: 'A novel low-firing microwave dielectric ceramic Li$_2$ZnGe$_3$O$_8$ with cubic spinel structure', *J. Eur. Ceram. Soc.*, 2017, **37**, (2), pp. 625–629

[15] Zhou, Y.Y., Tian, C.L., Meng, S.Q.*, et al.*: 'Structural transitions and microwave dielectric properties of Ba$_{2-2x}$Sr$_{2x}$SmSbO$_6$ double perovskites', *J. Am. Ceram. Soc.*, 2012, **95**, (5), pp. 1665–1670

[16] Mao, M.M., Chen, X.M., Liu, X.Q.: 'Structure and microwave dielectric properties of solid solution in SrLaAlO$_4$–Sr$_2$TiO$_4$ system', *J. Am. Ceram. Soc.*, 2011, **94**, pp. 3948–3952

[17] Zhang, Y., Zhang, Y.C., Xiang, M.Q.: 'Crystal structure and microwave dielectric characteristics of Zr-substituted CoTiNb$_2$O$_8$ ceramics', *J. Eur. Ceram. Soc.*, 2016, **36**, (8), pp. 1945–1951

[18] Zhang, J.J., Zhai, J.W., Chou, X.J.*, et al.*: 'Microwave and infrared dielectric response of tunable Ba$_{1-x}$Sr$_x$TiO$_3$ ceramics', *Acta Mater.*, 2009, **57**, (15), pp. 4491–4499

[19] Zhou, Y.Y., Yue, Z.X., Meng, S.Q.: 'Structural transitions and microwave dielectric properties of (Ba,Sr)$_2$LnSbO$_6$ (Ln = La, Pr, Nd, Sm, Gd, Dy) double perovskites', *Ferroelectrics*, 2012, **435**, pp. 119–128

[20] Ichinose, N., Shimada, T.: 'Effect of grain size and secondary phase on microwave dielectric properties of Ba(Mg$_{1/3}$Ta$_{2/3}$)O$_3$ and Ba([Mg, Zn]$_{1/3}$Ta$_{2/3}$)O$_3$ systems', *J. Eur. Ceram. Soc.*, 2006, **26**, pp. 1755–1759

[21] Wang, Y., Zuo, R.Z.: 'A novel low-temperature fired microwave dielectric ceramic BaMg$_2$V$_2$O$_8$ with ultra-low loss', *J. Eur. Ceram. Soc.*, 2016, **36**, (1), pp. 247–251

[22] Akbas, M.A., Davies, P.K.: 'Ordering-induced microstructures and microwave dielectric properties of the Ba(Mg$_{1/3}$Nb$_{2/3}$)O$_3$–BaZrO$_3$ system', *J. Am. Ceram. Soc.*, 1998, **81**, pp. 670–676

[23] Bian, J.J., Wu, J.Y., Ubic, R.*, et al.*: 'Structural stability and microwave dielectric properties of $(1-x)$Ba(Mg$_{1/2}$W$_{1/2}$)O$_3$–$x$Ba(RE$_{2/3}$W$_{1/3}$)O$_3$ (RE = Sm, Dy, Y, Yb) solid solutions', *J. Eur. Ceram. Soc.*, 2015, **35**, (5), pp. 1431–1439

[24] Song, K.X., Liu, P., Lin, H.X.*, et al.*: 'Symmetry of hexagonal ring and microwave dielectric properties of (Mg$_{1-x}$Ln$_x$)$_2$Al$_4$Si$_5$O$_{18+x}$ (Ln = La, Sm) cordierite-type ceramics', *J. Eur. Ceram. Soc.*, 2016, **36**, (5), pp. 1167–1175

[25] Xu, Y., Fu, R.L., Agathopoulos, S.*, et al.*: 'Synthesis and microwave dielectric properties of BaO–Sm$_2$O$_3$–5TiO$_2$ ceramics with NdAlO$_3$ additions', *Ceram. Int.*, 2016, **42**, (13), pp. 14573–14580

[26] Samal, S.L., Rao, G.L.N., Raju, K.C.J.*, et al.*: 'Microwave dielectric properties of new complex perovskites: (Ba$_{1/3}$Ln$_{2/3}$)(Zn$_{1/3}$Ti$_{2/3}$)O$_3$ (Ln = La, Pr, and Nd) and (Ba$_{(1+x)/3}$La$_{(2-x)/3}$)(Zn$_{1/3}$Ti$_{(2-x)/3}$Nb$_{x/3}$)O$_3$', *Jpn. J. Appl. Phys.*, 2009, **48**, p. 061401

[27] Dias, A., Matinaga, F.M., Moreira, R.L.: 'Vibrational spectroscopy and electron–phonon interactions in microwave-hydrothermal synthesized Ba(Mn$_{1/3}$Nb$_{2/3}$)O$_3$ complex perovskites', *J. Phys. Chem. B*, 2009, **113**, pp. 9749–9755

[28] Bhalla, A.S., Guo, R., Roy, R.: 'The perovskite structure–a review of its role in ceramic science and technology', *Mater. Res. Innov.*, 2000, **4**, (1), pp. 3–26

[29] Tamazyan, R., Smaalen, S.: 'Quantitative description of the tilt of distorted octahedra in ABX$_3$ structures', *Acta Crystallogr. B*, 2007, **63**, pp. 190–200

[30] Lufaso, M.W.: 'Crystal structures, modeling, and dielectric property relationships of 2:1 ordered Ba$_3$MM$'_2$O$_9$ (M = Mg, Ni, Zn; M$'$ = Nb, Ta) perovskites', *Chem. Mater.*, 2004, **16**, pp. 2148–2156

[31] Janaswamy, S., Murthy, G.S., Dias, E.D.*, et al.*: 'Ordering in BaMg$_{1/3}$Ta$_{1/3}$Nb$_{1/3}$O$_3$ ceramics: an X-ray rietveld analysis', *Crystallogr. Rep.*, 2006, **51**, pp. 231–235

[32] Burton, B.P.: 'Why Pb(B$_{1/3}$B$'_{2/3}$)O$_3$ perovskites disorder more easily than Ba(B$_{1/3}$B$'_{2/3}$)O$_3$ perovskites and the thermodynamics of 1:1-type short-range order in PMN', *J. Phys. Chem. Solids*, 2000, **61**, pp. 327–333

[33] Goodenough, J.B., Longo, J.M.: '*Crystallographic and magnetic properties of perovskite and perovskite-related compounds: new series*', vol. **4a**, (Springer, Berlin, 1970)

[34] Rao, C.N., Gopalakrishnan, J.: '*New directions in solid state chemistry: structure, synthesis, properties, reactivity, and materials*' (Cambridge University Press, Cambridge, 1986)

[35] Barker, A.S.: 'Temperature dependence of transverse and longitudinal optic mode frequencies and charges in SrTiO$_3$ and BaTiO$_3$', *Phys. Rev.*, 1966, **145**, pp. 391–399

[36] Lee, H.J., Park, H.M., Song, Y.W.*, et al.*: 'Microstructure characterizations in calcium magnesium niobate', *J. Am. Ceram. Soc.*, 2001, **84**, pp. 1632–1636

[37] Nagai, T., Sugaiyama, M., Sando, M.: 'Anomaly in the infrared active phonon modes and its relationship to the dielectric constant of (Ba$_{1-x}$Sr$_x$)(Mg$_{1/3}$Ta$_{2/3}$)O$_3$ compound', *Jpn. J. Appl. Phys.*, 1996, **35**, pp. 5163–5167

[38] Glazer, A.M.: 'The classification of tilted octahedra in perovskites', *Acta Crystallogr. B*, 1972, **28**, pp. 3384–3392

[39] Aleksandrov, K.S.: 'The sequences of structural phase transitions in perovskites', *Ferroelectrics*, 1976, **14**, pp. 801–805

[40] Reaney, I.M., Colla, E.L., Setter, N.: 'Dielectric and structural characteristics of Ba- and Sr-based complex perovskites as a function of tolerance factor', *Jpn. J. Appl. Phys.*, 1994, **33**, pp. 3984–3990

[41] Nagai, T., Sugiyama, M., Sando, M.*, et al.*: 'Structural changes in Ba(Sr$_{1/3}$Ta$_{2/3}$)O$_3$-type perovskite compounds upon tilting of oxygen octahedra', *Jpn. J. Appl. Phys.*, 1997, **36**, pp. 1146–1153

[42] Lee, H.J., Park, H.M., Song, Y.W.*, et al.*: 'Microstructure and dielectric properties of barium strontium magnesium niobate', *J. Am. Ceram. Soc.*, 2001, **84**, pp. 2105–2110

[43] Dong, H.L., Shi, F.: 'Vibration spectra and structural characteristics of Ba[(Zn$_{1-x}$Mg$_x$)$_{1/3}$Nb$_{2/3}$]O$_3$ solid solutions', *Appl. Spectrosc. Rev.*, 2011, **46**, pp. 207–221

[44] Takahashi, T., Wu, E.J., Ven, A.V.D.*, et al.*: 'First-principles investigation of B-site ordering in Ba(Mg$_x$Ta$_{1-x}$)O$_3$ microwave dielectrics with the complex perovskite structure', *Jpn. J. Appl. Phys.*, 2000, **39**, pp. 1241–1248

[45] Siny, I.G., Tao, R.W., Katiyar, R.S.*, et al.*: 'Raman spectroscopy of Mg–Ta order–disorder in BaMg$_{1/3}$Ta$_{2/3}$O$_3$', *J. Phys. Chem. Solids*, 1998, **59**, pp. 181–195

[46] Galasso, F.: '*Structure, properties, and preparation of perovskite-type compounds*' (Pergamon, New York, 1969)

[47] Wang, C.H., Jing, X.P., Wang, L.*, et al.*: 'XRD and Raman studies on the ordering/disordering of Ba(Mg$_{1/3}$Ta$_{2/3}$)O$_3$', *J. Am. Ceram. Soc.*, 2009, **92**, pp. 1547–1551

[48] Cheng, H.F., Chia, C.T., Liu, H.L.*, et al.*: 'Correlation of the phonon characteristics and microwave dielectric properties of the Ba(Mg$_{1/3}$Ta$_{2/3}$)O$_3$ materials', *J. Eur. Ceram. Soc.*, 2007, **27**, pp. 2893–2897

[49] Chen, Y.C., Cheng, H.F., Liu, H.L.*, et al.*: 'Correlation of microwave dielectric properties and normal vibration modes of $x$Ba(Mg$_{1/3}$Ta$_{2/3}$)O$_3$–$(1-x)$Ba(Mg$_{1/3}$Nb$_{2/3}$)O$_3$ ceramics: II. Infrared spectroscopy', *J. Appl. Phys.*, 2003, **94**, pp. 3365–3370

[50] Moreira, R.L., Andreeta, M.R.B., Hernandes, A.C.*, et al.*: 'Polarized micro-Raman spectroscopy of Ba(Mg$_{1/3}$Ta$_{2/3}$)O$_3$ single crystal fibers', *Cryst. Growth Des.*, 2005, **5**, pp. 1457–1462

[51] Moreira, R.L., Matinaga, F.M., Dias, A.: 'Raman-spectroscopic evaluation of the long-range order in Ba(B$'_{1/3}$B$''_{2/3}$)O$_3$ ceramics', *Appl. Phys. Lett.*, 2001, **78**, pp. 428–430

[52] Shi, F., Dong, H.: 'Correlation of crystal structure, dielectric properties and lattice vibration spectra of (Ba$_{1-x}$Sr$_x$)(Zn$_{1/3}$Nb$_{2/3}$)O$_3$ solid solutions', *Dalton Trans.*, 2011, **40**, pp. 6659–6667

[53] Chen, M.Y., Chia, C.T., Lin, I.N.*, et al.*: 'Microwave properties of Ba(Mg$_{1/3}$Ta$_{2/3}$)O$_3$, Ba(Mg$_{1/3}$Nb$_{2/3}$)O$_3$ and Ba(Co$_{1/3}$Nb$_{2/3}$)O$_3$ ceramics revealed by Raman scattering', *J. Eur. Ceram. Soc.*, 2006, **26**, pp. 1965–1968

[54] Wang, C.H., Kuang, X.J., Jing, X.P.*, et al.*: 'Far infrared reflection spectrum and IR-active modes of MgTiO$_3$', *J. Appl. Phys.*, 2008, **103**, p. 074105

[55] Dias, A., Moreira, R.L.: 'Far-infrared spectroscopy in ordered and disordered BaMg$_{1/3}$Nb$_{2/3}$O$_3$ microwave ceramics', *J. Appl. Phys.*, 2003, **94**, pp. 3414–3421

[56] Sagala, D.A., Koyasu, S.: 'Infrared reflection of Ba(Mg$_{1/3}$Ta$_{2/3}$)O$_3$ ceramics', *J. Am. Ceram. Soc.*, 1993, **76**, pp. 2433–2436

[57] Cochran, W.: '*The dynamics of atoms in crystals*' (Edward Arnold, London, 1973)

[58] Born, M., Huang, K.: '*Dynamical theory of crystal lattices*' (Oxford University Press, London, 1954)

[59] Farmer, V.C., Lazarev, A.N.: 'Symmetry and crystal vibrations', in Farmer, V.C. (Ed.): '*The infrared spectra of minerals*' (Bartholomew Press, London, 1974), pp. 51–67

[60] Wang, C.H., Liu, G.H., Jing, X.P.*, et al.*: 'First-principle calculation and far infrared measurement for infrared-active modes of Ba(Mg$_{1/3}$Ta$_{2/3}$)O$_3$', *J. Am. Ceram. Soc.*, 2010, **93**, pp. 3782–3787

[61] Decicco, P.D., Johnson, F.A.: 'Quantum theory of lattice dynamics', *Proc. R. Soc. Lond. A, Math. Phys. Sci.*, 1969, **310**, pp. 111–116

[62]  Fateley, W.G., Dollish, F.R., McDevitt, N.T., *et al.*: '*Infrared and Raman selection rules for molecular and lattice vibrations: the correlation method*' (John Wiley & Sons, Inc., USA, 1972)

[63]  Wang, C.H., Jing, X.P., Feng, W., *et al.*: 'Assignment of Raman-active vibrational modes of $MgTiO_3$', *J. Appl. Phys.*, 2008, **104**, p. 034112

[64]  Kroumova, E., Aroyo, M.I., Perez-Mato, J.M., *et al.*: 'Bilbao crystallographic server: useful databases and tools for phase-transition studies', *Phase Transit.*, 2003, **76**, pp. 155–170

[65]  Damen, T.C., Porto, S.P.S., Tell, B.: 'Raman effect in zinc oxide', *Phys. Rev.*, 1966, **142**, pp. 570–574

[66]  Pezzotti, G.: 'Raman spectroscopy of piezoelectrics', *J. Appl. Phys.*, 2013, **113**, p. 211301

[67]  Lin, I.N., Chia, C.T., Liu, H.L., *et al.*: 'High frequency dielectric properties of $Ba(Mg_{1/3}Ta_{2/3})O_3$ complex perovskite ceramics', *J. Eur. Ceram. Soc.*, 2003, **23**, pp. 2633–2637

[68]  Gervais, F., Piriou, B.: 'Temperature dependence of transverse-optic and longitudinal-optic modes in $TiO_2$ (Rutile)', *Phys. Rev. B*, 1974, **10**, pp. 1642–1654

[69]  Rivier, N.: 'Theory of crystal space groups and infra-red and Raman lattice processes of insulating crystals', *J. Mod. Opt.*, 1976, **23**, pp. 167–168

[70]  Tao, R., Siny, I.G., Katiyar, R.S., *et al.*: 'Temperature-dependent Raman studies of $Ba(Mg_{1/3}Ta_{2/3})O_3$', *J. Raman Spectrosc.*, 1996, **27**, pp. 873–877

[71]  Tamura, H., Sagala, D.A., Wakino, K.: 'Lattice vibrations of $Ba(Zn_{1/3}Ta_{2/3})O_3$ crystal with ordered perovskite structure', *Jpn. J. Appl. Phys.*, 1986, **25**, pp. 787–791

[72]  Chia, C.T., Chen, Y.C., Cheng, H.F.: 'Correlation of microwave dielectric properties and normal vibration modes of $Ba(Mg_{1/3}Ta_{2/3O_3}–(1-x)Ba(Mg_{1/3}Nb_{2/3})O_3$ ceramics: I. Raman spectroscopy', *J. Appl. Phys.*, 2003, **94**, pp. 3360–3364

[73]  Diao, C.L., Wang, C.H., Luo, N.N., *et al.*: 'First- principle calculation and assignment for vibrational spectra of $Ba(Mg_{1/3}Nb_{2/3})O_3$ microwave dielectric ceramic', *J. Appl. Phys.*, 2014, **115**, p. 114103

[74]  Poulet, H., Mathieu, J.P.: '*Vibration spectra and symmetry of crystals*' (Cordon and Breach, New York, 1976), pp. 326, 498, 519 (translated by A. Simievic)

[75]  Harris, D.C., Bertolucci, M.D.: '*Symmetry and spectroscopy: an introduction to vibrational and electronic spectroscopy*' (Oxford University Press, New York, 1978), pp. 170–173

[76]  Dias, A., Paschoal, C.W.A., Moreira, R.L.: 'Infrared spectroscopic investigations in ordered barium magnesium niobate ceramics', *J. Am. Ceram. Soc.*, 2003, **86**, pp. 1985–1987

[77]  Shi, F., Dong, H.L.: 'Correlation between vibrational modes and structural characteristics of $Ba[(Zn_{1-x}Mg_x)_{1/3}Ta_{2/3}]O_3$ solid solutions', *CrystEngComm*, 2012, **14**, pp. 3373–3379

[78]  Shi, F., Dong, H.L.: 'Correlation of the phonon characteristics and crystal structure of $Ba[Zn_{1/3}(Nb_{1-x}Ta_x)_{2/3}]O_3$ solid solutions', *J. Appl. Phys.*, 2012, **111**, p. 014111

[79]  Payne, M.C., Teter, M.P., Allan, D.C., *et al.*: 'Iterative minimization techniques for ab initio total-energy calculations molecular- dynamics and conjugate gradients', *Rev. Mod. Phys.*, 1992, **64**, pp. 1045–1097

[80]  Dai, Y.D., Zhao, G.H., Guo, L.L., *et al.*: 'First-principles study of the difference in permittivity between $Ba(Mg_{1/3}Ta_{2/3})O_3$ and $Ba(Mg_{1/3}Nb_{2/3})O_3$', *Solid State Commun.*, 2009, **149**, pp. 791–794

[81]  Dias, A., Franklin, M.M., Roberto, L.M.: 'Raman spectroscopy of $(Ba_{1-x}Sr_x)(Mg_{1/3}Nb_{2/3})O_3$ solid solutions from microwave-hydrothermal powders', *Chem. Mater.*, 2007, **19**, pp. 2335–2341

[82]  Venkatesh, J., Subramanian, V., Murthy, V.R.K.: 'Far-IR reflectance study on $(Ba_{1-x}Sr_x)(Zn_{1/3}Ta_{2/3})O_3$ dielectric resonators as a function of tolerance factor', *Physica B, Condens. Matter*, 2000, **293**, pp. 118–124

[83]  Zhang, H., Diao, C.L., Liu, S.L., *et al.*: 'X-ray diffraction and Raman scattering investigations on $Ba[Mg_{(1-x)/3}Zr_xTa_{2(1-x)/3}]O_3$ solid solutions', *J. Alloys Compd.*, 2014, **587**, pp. 717–723

[84]  Zhang, H., Diao, C.L., Liu, S.L., *et al.*: 'XRD and Raman studies on crystal structures and dielectric properties of $Ba[Mg_{(1-x)/3}Zr_xNb_{2(1-x)/3}]O_3$ solid solutions', *Ceram. Int.*, 2014, **4**, pp. 2427–2434

[85]  Shi, F., Dong, H.L.: 'Vibrational modes and structural characteristics of $(Ba_{0.3}Sr_{0.7})[(Zn_xMg_{1-x})_{1/3}Nb_{2/3}]O_3$ solid solutions', *Dalton Trans.*, 2011, **40**, pp. 11591–11598

[86]  Lee, H.J., Park, H.M., Song, Y.W., *et al.*: 'Microstructural characteristics of strontium magnesium niobate', *J. Am. Ceram. Soc.*, 2001, **84**, pp. 3032–3036

[87]  Kim, B.K., Hamaguchi, H., Kim, I.T., *et al.*: 'Probing of 1:2 ordering in $Ba(Ni_{1/3}Nb_{2/3})O_3$ and $Ba(Zn_{1/3}Nb_{2/3})O_3$ ceramics by XRD and Raman spectroscopy', *J. Am. Ceram. Soc.*, 1995, **78**, pp. 3117–3120

[88]  Webb, S.J., Breeze, J., Scott, R.I., *et al.*: 'Raman spectroscopic study of gallium-doped Ba $(Zn_{1/3}Ta_{2/3})$ O $_3$', *J. Am. Ceram. Soc.*, 2002, **85**, pp. 1753–1756

[89]  Dias, A., Giminelli, V.S.T., Matinagaa, F.M., *et al.*: 'Raman scattering and X-ray diffraction investigations on hydrothermal barium magnesium niobate ceramics', *J. Eur. Ceram. Soc.*, 2001, **21**, pp. 2739–2744

[90]  Lee, C.C., Chou, C.C., Tsai, D.S.: 'Variation in the ordering of $Ba(Zn_{1/3}Ta_{2/3})O_3$ with A-site substitutions', *Ferroelectrics*, 1998, **206**, pp. 293–305

[91]  Diao, C.L., Shi, F.: 'Effects of sintering temperatures on dielectric properties, vibrational modes and crystal structures in $Ba[(Ni_{0.7}Zn_{0.1})]_{1/3}Nb_{2/3}]O_3$ ceramics', *J. Mater. Sci.*, 2012, **47**, pp. 5438–5445

[92]  Dong, H.L., Shi, F.: 'Effect of synthesis temperature on crystal structure and phonon modes of $Ba[Zn_{1/3}(Nb_{0.4}Ta_{0.6})_{2/3}]O_3$ ceramics', *CrystEngComm*, 2012, **14**, pp. 8268–8273

[93]  Wei, D.M., Dong, H.L., Zhang, H., *et al.*: 'Correlation between crystal structures and vibration modes of $Ba[(Zn_{1-x}Mg_x)_{1/3}Nb_{2/3}]O_3$ ceramics as a function of sintering temperatures', *J. Mater. Sci., Mater. Electron.*, 2014, **25**, pp. 2748–2758

[94]  Qiao, M.H., Bian, Y.J., Qi, G.H., *et al.*: 'Effects of sintering temperatures on dielectric properties, vibrational modes and crystal structures in $Ba[Sn_{0.32}Zn_{0.68/3}Nb_{1.36/3}]O_3$ ceramics', *J. Mater. Sci., Mater. Electron.*, 2014, **25**, pp. 4129–4138

[95]  Diao, C.L., Shi, F.: 'Correlation among dielectric properties, vibrational modes and crystal structures in $Ba[Sn_xZn_{(1-x)/3}Nb_{2(1-x)/3}]O_3$ solid solutions', *J. Phys. Chem. C*, 2012, **116**, pp. 6852–6858

[96]  Jiang, S.Z., Yue, Z.X., Shi, F.: 'Effects of $BaWO_4$ additive on Raman phonon modes and structure–property relationship of $Ba(Mg_{1/3}Ta_{2/3})O_3$ microwave dielectric ceramics', *J. Alloys Compd.*, 2015, **646**, pp. 49–55

[97]  Wang, L., Zhang, H., Leng, Y., *et al.*: 'Effects of $CaTiO_3$ on crystal structures and dielectric properties of $Ba(Zn_{1/3}Nb_{2/3})O_3$ ceramics via X-ray diffraction and Raman spectroscopy', *J. Mater. Sci., Mater. Electron.*, 2014, **25**, pp. 3403–3411

[98]  Liang, K., Shi, F., Liu, H.Q., *et al.*: 'Far infrared reflection study on structure–property relationship of $Ba[Mg_{(1-x)/3}Zr_xTa_{2(1-x)/3}]O_3$ ceramics', *J. Mater. Sci., Mater. Electron.*, 2016, **27**, (1), pp. 800–805

[99]  Wakino, K., Murata, M., Tamura, H.: 'Far-infrared reflection spectra of $Ba(Zn,Ta)O_3$–$BaZrO_3$ dielectric resonator material', *J. Am. Ceram. Soc.*, 1986, **69**, pp. 34–37

[100]  Fukuda, K., Kitoh, R., Awai, I.: 'Far-infrared reflection spectra of dielectric ceramics for microwave applications', *J. Am. Ceram. Soc.*, 1994, **77**, pp. 149–154

[101]  Shimada, T.: 'Far-infrared reflection and microwave properties of $Ba([Mg_{1-x}Zn_x]_{1/3},Ta_{2/3})O_3$ ceramics', *J. Eur. Ceram. Soc.*, 2004, **24**, pp. 1799–1803

[102]  Dai, Y.D., Zhao, G.H., Liu, H.X.: 'First-principles study of the dielectric properties of $Ba(Zn_{1/3}Nb_{2/3})O_3$ and $Ba(Mg_{1/3}Nb_{2/3})O_3$', *J. Appl. Phys.*, 2009, **105**, p. 034111

[103]  Shi, F., Gu, Y.F., Li, C.X.: 'Fourier transform far-infrared reflection spectroscopy of $Ba[Zn_{1/3}(Nb_{1-x}Ta_x)_{2/3}]O_3$ solid solutions', *Adv. Mater. Res.*, 2014, **873**, pp. 316–321

[104]  Yue, Z.X., Shi, F., Gu, Y.F., *et al.*: 'Far-infrared reflection study of $Ba[Mg_{(1-x)/3}Zr_xNb_{2(1-x)/3}]O_3$ microwave dielectric ceramics', *Sci. Sin. Tech.*, 2014, **44**, pp. 1247–1253

[105]  Spitzer, W.G., Miller, R.C., Kleinmam, D.A., *et al.*: 'Far infrared dielectric dispersion in $BaTiO_3$, $SrTiO_3$, and $TiO_2$', *Phys. Rev.*, 1962, **126**, pp. 1710–1721

[106]  Perry, C.H., McCarthy, D.J., Rupprecht, G.: 'Dielectric dispersion of some perovskite zirconate', *Phys. Rev. A*, 1965, **138**, pp. 1537–1538

[107]  Roessler, D.M.: 'Kramers–Kronig analysis of reflection data', *Br. J. Appl. Phys.*, 1965, **16**, pp. 1119–1123

[108]  Roessler, D.M.: 'Kramers–Kronig analysis of non-normal incidence reflection', *Br. J. Appl. Phys.*, 1965, **16**, pp. 1359–1367

[109]  Nakagawa, I.: '*Shindo Bunkogaku (vibrational spectroscopy)*' (Gakkaishuppan-Center, Tokyo, 1987), p. 205 [in Japanese]

[110]  Venkatesh, J., Sivasubramanian, V., Subramanian, V., *et al.*: 'Far IR reflectance study on B-site disordered $Ba(Zn_{1/3}Ta_{2/3})O_3$ dielectric resonator', *Mater. Res. Bull.*, 2000, **35**, pp. 1325–1332

[111]  Venkatesh, J., Subramanian, V., Murthy, V.R.K.: 'Far-IR reflectance study on $(Ba_{1-x})Sr_x)(Zn_{1/3}Ta_{2/3})O_3$ dielectric resonators as a function of tolerance factor', *Physica B, Condens. Matter*, 2000, **293**, pp. 118–124

[112]  Sawada, A., Kuwabara, T.: 'Infrared study of $Ba(Mg_{1/3}Ta_{2/3})O_3$ ceramics for microwave resonator', *Ferroelectrics*, 1989, **95**, pp. 205–208

[113]  Zhou, D., Pang, L.X., Wang, H., *et al.*: 'Phase transition, Raman spectra, infrared spectra, band gap and microwave dielectric properties of low temperature firing $(Na_{0.5x}Bi_{1-0.5x})(Mo_xV_{1-x})O_4$ solid solution ceramics with scheelite structures', *J. Mater. Chem.*, 2011, **21**, (45), pp. 18412–18420

[114]  Xi, H.H., Zhou, D., Xie, H.D., *et al.*: 'Raman spectra, infrared spectra, and microwave dielectric properties of low-temperature firing $[(Li_{0.5}Ln_{0.5})_{1-x}Ca_x]MoO_4$ (Ln = Sm and Nd) solid solution ceramics with scheelite structure', *J. Am. Ceram. Soc.*, 2015, **98**, (2), pp. 587–593

[115]  Kamba, S., Hughes, H., Noujni, D., *et al.*: 'Relationship between microwave and lattice vibration properties in $Ba(Zn_{1/3}Nb_{2/3})O_3$-based microwave dielectric ceramics', *J. Phys. D, Appl. Phys.*, 2004, **37**, (14), p. 1980

[116]  Pashkin, A., Kamba, S., Berta, M., *et al.*: 'High frequency dielectric properties of $CaTiO_3$-based microwave ceramics', *J. Phys. D, Appl. Phys.*, 2005, **38**, (5), p. 741

[117]  Petzelt, J., Pačesová, S., Fousek, J., *et al.*: 'Dielectric spectra of some ceramics for microwave applications in the range of 1010–1014 Hz', *Ferroelectrics*, 1989, **93**, (1), pp. 77–85

[118]  Gervais, F., Piriou, B.: 'Temperature dependence of transverse- and longitudinal-optic modes in $TiO_2$, (Rutile)', *Phys. Rev. B*, 1980, **10**, p. B203841

[119]  Dong, H.L., Shi, F.: 'Effects of synthesis temperatures on crystal structures and lattice vibration modes of $(Ba_{0.3}Sr_{0.7})[(Zn_{1-x}Mg_x)_{1/3} Nb_{2/3}]O_3$ solid solutions', *Metall. Mater. Trans. A*, 2012, **43**, pp. 5128–5139

[120]  Woodward, P.M.: 'Octahedral tilting in perovskites. II. Structure stabilizing forces', *Acta Crystallogr. B*, 1997, **53**, pp. 32–43